Metabolomic characterization of behaviorally manipulated ants with multiomic data integration

I. Will[1*], G.M. Attardo[2], C. de Bekker[1,3*]

1: University of Central Florida, Biology Department, USA

2: University of California – Davis, Entomology and Nematology Department, USA

3: Utrecht University, Biology Department, NL

* Corresponding authors: ian.will@knights.ucf.edu (IW), a.m.debekker@uu.nl (CdB)

ORCiD: 0000-0002-2396-6778 (IW), 0000-0001-6265-2969 (GMD), 0000-0002-7325-172X (CdB)

Abstract

Parasitically manipulated *Camponotus floridanus* ants show multiple diseased behaviors and a fatal summiting phenotype when infected by *Ophiocordyceps camponoti-floridani* fungi. Altered host behavior as a response to and driven by parasites occur in a broad swath of taxa. In many cases, such as this interaction, the underlying mechanisms have not yet been clearly characterized. The drastic phenotypic changes observed could in some cases reflect large physiological changes within cells, spanning different molecular levels from nucleic acids to metabolites. Here, we link existing genomic and transcriptomic data to a new metabolomic dataset we produced to hypothesize on the mechanisms of manipulated "zombie ants" from a multiomic perspective. Multiple lines of evidence point toward dysregulation of neurotransmitters and neuronal signaling. We propose that these processes are altered during infection and manipulation based on: neurotransmitter synthesis and receptor gene expression, altered metabolite abundances, with plausible behavioral ties to known effects of these neurotransmitters in ants and other insects, and possible suppression of a connected immunity pathway. We additionally report signals for fungal metabolic activity during manipulation and early evidence for alterations of host processes related to detoxification, anti-stress protectants, and insect hormone metabolism.

Introduction

Hosts infected by parasites can show altered phenotypes that can be adaptive for the host or parasite. In the latter case, specifically promoted parasite-adaptive changes in host behavior are often referred to as parasitic behavioral manipulation. Examples of apparent manipulations of host behavior and physiology occur in a broad range of host and parasite taxa, although the underlying mechanisms are still being revealed (Thomas *et al.* 2010; Moore 2013; Heil 2016; Libersat *et al.* 2018; de Bekker *et al.* 2021).

In many parasitic manipulations, insect hosts succumb to summit disease, where the manipulated individual occupies an elevated location and dies in a stereotypical manner (Lovett *et al.* 2020; de Bekker *et al.* 2021). These final, elevated, exposed summit positions can be adaptive for the parasite by aiding transmission either by direct dispersal of the parasite or trophic transmission. As an example of the summit and disperse strategy, the ant-manipulating *Ophiocordyceps* (zombie ant fungi) have been leveraged in laboratory studies to better understand the mechanistic basis of behavioral manipulation. Manipulated ants display a summiting behavior, latching and biting onto their final summit perches until their death. Preceding this fatal change in behavior, infected ants also deviate from foraging trails and increase locomotor activity, reduce nestmate communication, and convulse (Pontoppidan *et al.* 2009; Andersen *et al.* 2009; Hughes *et al.* 2011; de Bekker *et al.* 2015; Sakolrak *et al.* 2018; Trinh *et al.* 2021).

Observed manipulation phenotypes likely do not hinge solely on activity by only the host or parasite. Rather, ant hosts may already demonstrate behaviors that can be easily coopted for manipulation by the fungal parasite. In this case, the parasite may benefit by taking advantage of and influencing host processes and symptoms without relying on costly mechanisms to “rewire” their hosts (Adamo 2019; Lovett *et al.* 2020). Although, deeper understanding of the fitness cost and benefits for both hosts and parasites may reveal that such behaviors could also be sometimes adaptive for hosts, at the individual or group level (perhaps especially so for eusocial animals, such as ants). Regardless of the ultimate “source” of manipulated behavior, physiological and molecular characterizations of hosts displaying modified behavior may offer a glimpse into how parasites (or hosts) modulate animal behavior, the coevolution of specialized host-parasite relationships, and undescribed properties of certain proteins and metabolites.

51 In the myrmecophilous *Ophiocordyceps*, investigations of phenotypes, genomes, transcriptomes,
52 and metabolomes continue to accumulate and help bring the most robust mechanistic hypotheses into
53 focus. The range of hypotheses touch upon: neuromodulators and effector proteins, circadian rhythms and
54 phototropism, insect hormones and behavioral-profile regulators, neuroprotectants, and muscular
55 hyperactivity (de Bekker *et al.* 2014a; Kobmoo *et al.* 2018; de Bekker 2019; Mangold *et al.* 2019; Zheng
56 *et al.* 2019; Loreto and Hughes 2019; Will *et al.* 2020; Trinh *et al.* 2021; de Bekker and Das 2022).
57 Previous metabolomic works centered on the *Ophiocordyceps kimflemingiae* zombie ant fungus have
58 already identified various metabolites associated with manipulation. These metabolomic signals also vary
59 in a species-specific manner, changing when either the parasite or host was a exchanged for a different
60 species (de Bekker *et al.* 2014b; Zheng *et al.* 2019; Loreto and Hughes 2019). Here, we continue to add to
61 these works in a "multiomic" approach with a new metabolomic analysis of *Camponotus floridanus*
62 (Florida carpenter ant) manipulated by *Ophiocordyceps camponoti-floridani* (Florida zombie ant fungus)
63 interpreted in the context of existing transcriptomic and genomic data (Will *et al.* 2020).
64 As the key processes of manipulation could involve specialized and general mechanisms, host
65 and parasite effectors, or changes from the genetic to chemical level, multiomic approaches cast a broad
66 net to improve detection. At the same time, combing these multiple approaches and datatypes can identify
67 consistent and robust signals for key biological processes. To supplement existing transcriptomic data, we
68 collected metabolomic data using three liquid chromatography-tandem mass spectrometry (LC-MS/MS)
69 protocols. We focused on altered metabolic pathways supported by a combination of metabolite and gene
70 signals. Similarly, we note when manipulation-associated metabolite features are selected by multiple
71 statistical methods. This approach follows the intuition that every analysis is subject to its own biases but
72 data that represent substantial biological changes are more likely to be selected by multiple
73 complementary tests.
74 Our study compared whole head samples of healthy *C. floridanus* ants and ants manipulated by
75 *O. camponoti-floridani*. Sampling whole heads allowed direct comparison to Will *et al.* 2020
76 transcriptomic ant-head data. Although metabolomic signals will be homogenized, whole heads will

77 contain the chemical profiles of ant neural tissue, muscle, and hemolymph in addition to fungal cells that
78 all may contain metabolites of most interest (Hughes *et al.* 2011; de Bekker *et al.* 2014b, 2015;
79 Fredericksen *et al.* 2017; Mangold *et al.* 2019; Zheng *et al.* 2019; Loreto and Hughes 2019). By analyzing
80 our metabolomic data in light of previous genomic and transcriptomic data, we propose multiple
81 pathways and compounds that reflect, or drive, manipulated behavior in *Ophiocordyceps* infected ants.
82

83 **Results & discussion**

84 **Infection mortality, observations of manipulation, and LC-MS/MS datasets:** Similar to
85 previous laboratory infections with *O. camponoti-floridani* (Will *et al.* 2020), *C. floridani* displaying
86 manipulated biting in this study were collected between 4 hr before to 0.5 hr after dawn, beginning three
87 weeks after infection (Fig. 1). Sham treatment healthy ants showed no mortality until 29 days post
88 injection (dpi), whereas infection treatment ants began to die immediately once we started recording
89 deaths on 4 dpi. This difference in survival was markedly different between treatments ($p = 4.1E-7$, log-
90 rank test) (Fig. 1A). In total, three sham treatment ants died out of the 28 (11%) that survived through 3
91 dpi. Twenty-three infected ants were manipulated out of the 39 (59%) that survived through 3 dpi. The
92 other 16 infected ants died with visible blastospore loads but without observed behavioral manipulation.
93 In total, these experimental infections produced 20 manipulated ants, 20 healthy (sham) ants, and
94 three blank-collection samples produced from the ant housing of the sham treatment (Fig. 2A). From
95 these samples, we produced three LC-MS/MS datasets, "biogenic amines," "polyphenols," and "lipids,"
96 containing 2,955, 4,315, and 4,924 analyzed features, respectively. (Fig. 2A-B).
97
98
99

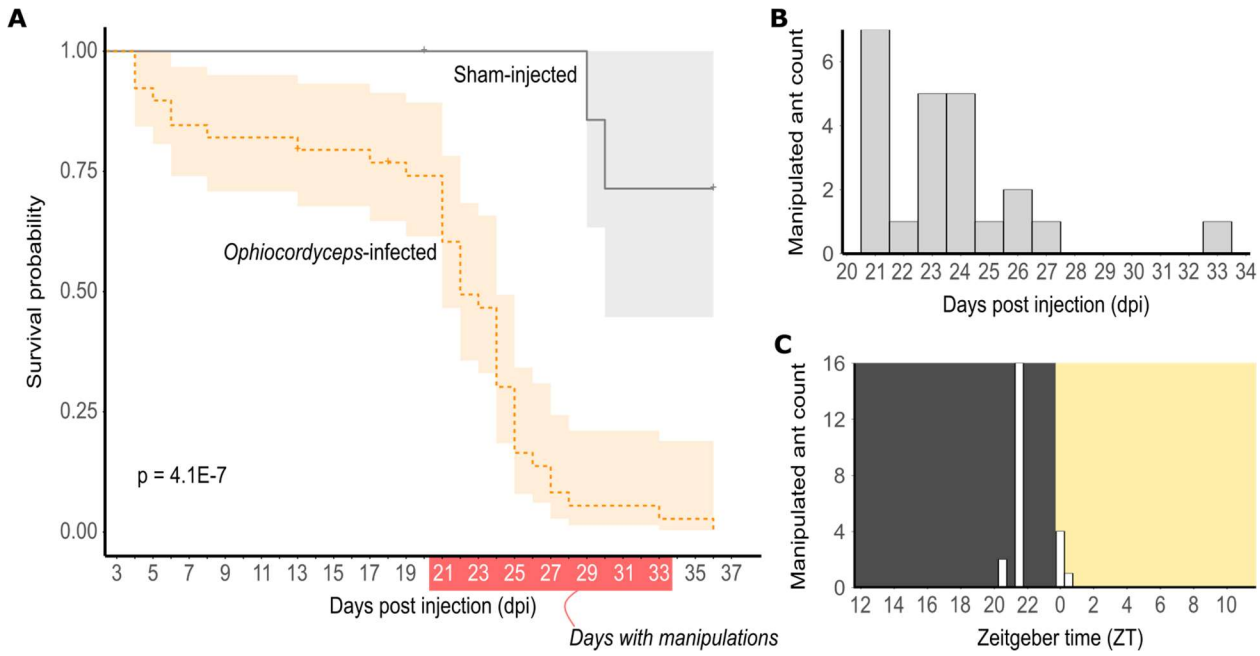

Figure 1. Ant manipulations occur at stereotypical days and times.
A) *O. camponoti-floridani* infection leads to significantly increased mortality compared to sham treatment (p = 4.1E-7, log-rank test). B) Manipulated ants most often appeared 21-27 dpi, but as late as 33 dpi. C) Manipulated ants were collected near dawn, most often at ZT 21.5, 2.5 hr before lights turned on.

Metabolomic feature selection and grouping for pathway enrichment analyses: After data quality control and filtering (Fig. 2B), we constructed a set of features for study-wide pathway enrichment analysis that distinguished healthy and manipulated ants by: categorization as differentially abundant metabolites (DAMs), loading values in principal component analyses (PCAs), and importance for navigating decision trees (Boruta) (Kursa and Rudnicki 2010) (Fig. 2C). Combining all three LC-MS/MS datasets, approximately 60% of features were DAMs, with most DAMs increasing in abundance in manipulated ants compared to healthy controls (Fig. 3A, Table 5). Separation of treatment groups by PCA only clearly clustered along PC1 (ca. 60% to 80%), with PC2 (ca. 4% to 9%) and other PCs (not shown) describing little of the variation between treatments (Fig. 3B). Using Boruta random forests, we found ca. 40% of features to be “confirmed” as “important” for distinguishing treatment types (Table 5). We performed pathway analyses with a study-wide group of features that satisfied at least

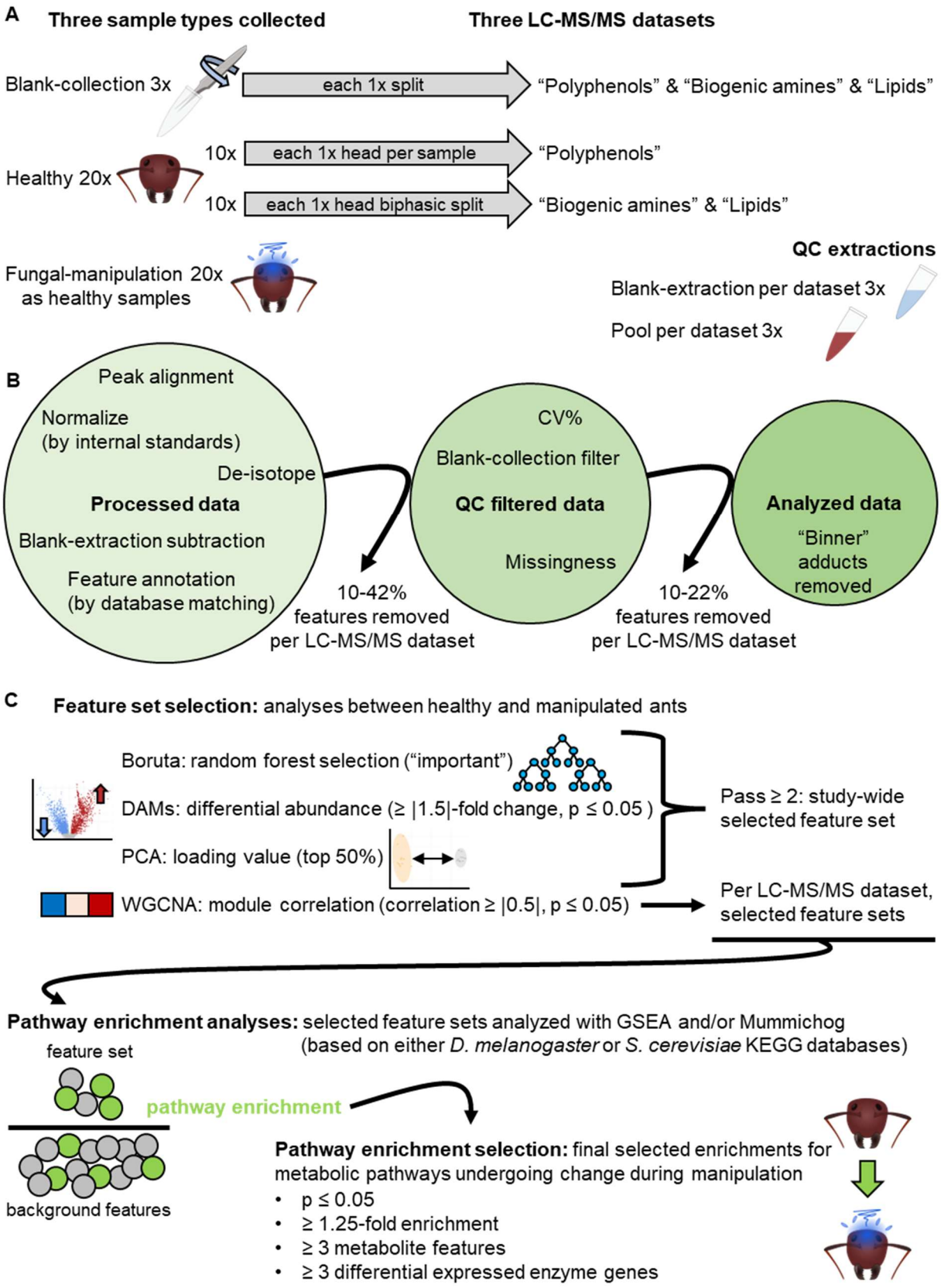

Figure 2. Experimental overview and analytical framework for enrichment analyses.

118 A) Three types of experimental samples were collected, blank-collections (mock sampling using tools and ant
119 housing for healthy ants), healthy ants (given sham-injections only), and manipulated ants (infected with
120 *Ophiocordyceps* and displaying manipulation phenotypes). The metabolomics core facility introduced two quality
121 control (QC) extractions. First, blank-extractions using core facility materials only (and therefore distinct from
122 experimental blank-collections). Second, pooled extractions of all samples used for a given LC-MS/MS dataset.
123 Three LC-MS/MS datasets were produced, each being an untargeted analysis but tailored to different chemistries to
124 collect broad data overall. B) The metabolomics core generated "Processed data" from which we produced "QC
125 filtered data" and "Analyzed data" by applying quality control and data reduction steps. C) We used multiple
126 statistical tests to select features of interest for metabolic pathway enrichment analyses. Results from those
127 enrichment analyses were subsequently subjected to multiple filters to arrive at a final set of pathways and feature
128 sets of interest. Full details on these samples and approaches are given in Methods.
129

130 two of following criteria: (*i*) it was a DAM, (*ii*) it was among the highest 50% of absolute PC1 loading
131 values, or (*iii*) it was confirmed by Boruta. Most features that satisfied at least two requirements (n =
132 6,468 features, 53% of a total 12,194 features), in fact satisfied all three (n = 4,656, 72% of features
133 passing two criteria) (Fig. 2C, 15C, Supp. Table 1, Supp. Data 1). The feature set passing at least two
134 filters contained 347 of the 760 (46%) features given compound annotations by the WCMC. The many
135 features passing our filters is likely due to a combination of metabolites related specifically to infection
136 processes and general aspects of fungal metabolism, as *O. camponti-floridani* cells were only present in
137 manipulated ants. For this set of features passing at least two selection filters, we jointly analyzed them
138 with Mummichog and a gene set enrichment analysis (GSEA)-based approach in MetaboAnalyst for
139 enriched metabolic pathways found in the Kyoto Encyclopedia of Genes and Genomes (KEGG) (Fig. 2C)
140 (Kanehisa and Goto 2000; Li *et al.* 2013; Pang *et al.* 2021). We detected eight significantly enriched
141 pathways that passed our p-value, minimum metabolite feature, fold-enrichment, and enzyme
142 differentially expressed gene (DEG) thresholds (Fig. 2C, Table 6, Supp. Data 2). These enzyme DEGs use
143 previously published expression data from an *Ophiocordyceps* manipulation study (Will *et al.* 2020) and
144 were associated here with their respective KEGG metabolic pathways. Most enzyme DEGs were
145 downregulated both in the ant (90%) and the fungus (62%). This degree of downregulation is higher than
146 previously found for transcriptome-wide DEGs during manipulation (Will *et al.* 2020) (Supp. File 1).

147

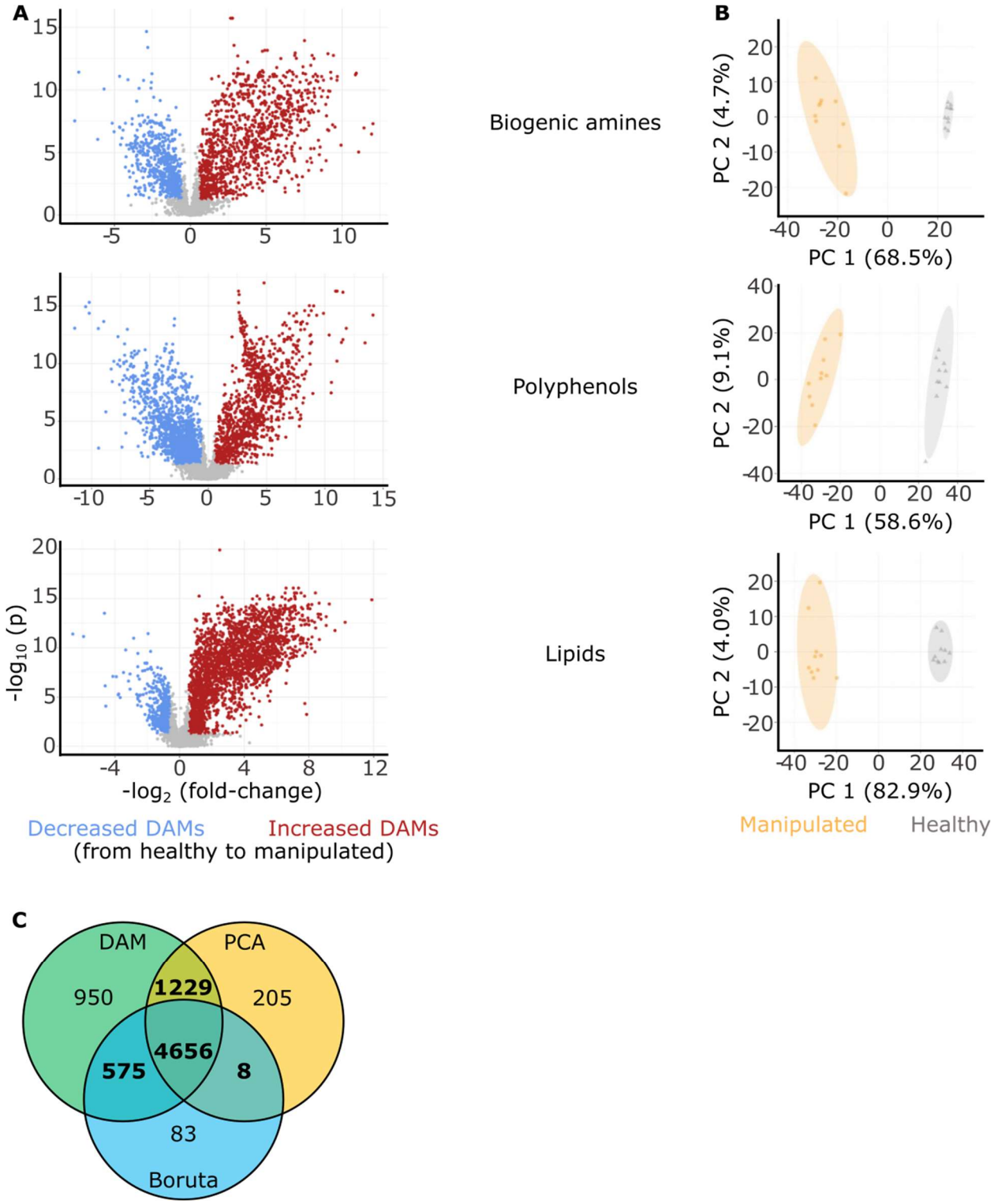

148

149 **Figure 3. Feature selection overview.**

150 A) Volcano plots per dataset show DAMs that increased (red) or decreased (blue) at manipulation according to a 1.5-

151 fold change and $p \leq 0.05$. B) PCAs for each dataset show distinct clustering of samples between manipulated (orange)
152 and healthy ants (gray) along PC1. C) Features that passed at least two selection criteria (bold) were used for study-
153 wide pathway analyses. We used DAM analyses to select features as described above, PCAs to select features in the
154 top 50% of PC 1 loading values, and the Boruta analysis to select features identified as "important."
155
156 **Table 1. All enriched KEGG pathways selected across analyzed feature sets.**
157 KEGG pathways that were found in Mummichog or GSEA analyses ($p \leq 0.05$) also were required to show a
158 minimum 1.25-fold enrichment, three features contributing to that enrichment, and three DEGs that were
159 homologous to representative enzyme genes within that pathway. Each pathway is listed alphabetically once in the
160 table, with all feature sets (network modules or the study-wide feature set that passed at least two selection filters)
161 that were enriched for that pathway.

Enriched KEGG metabolic pathway	**Feature sets**					
Alanine, aspartate and glutamate metabolism	P13					
Amino sugar and nucleotide sugar metabolism	A1	P1	P2	P3	P18	study-wide
Aminoacyl-tRNA biosynthesis	L3	P2	P11			
Arginine and proline metabolism	A1	P2				
Arginine biosynthesis	A1					
Ascorbate and aldarate metabolism	A1	P13				
beta-Alanine metabolism	P2	study-wide				
Biosynthesis of unsaturated fatty acids	L2	L10	P3	study-wide		
Butanoate metabolism	P2					
Citrate cycle (TCA cycle)	P3	P13				
Cyanoamino acid metabolism	A1					
Cysteine and methionine metabolism	L1	P1	P18			
Drug metabolism - cytochrome P450	L3	P3				
Drug metabolism - other enzymes	A1	study-wide				
Fatty acid degradation	P3					
Folate biosynthesis	P2					
Fructose and mannose metabolism	P2	P18				
Galactose metabolism	A1	P18	study-wide			
Glutathione metabolism	A1					
Glycerolipid metabolism	P2					
Glycerophospholipid metabolism	P2	study-wide				
Glycine, serine and threonine metabolism	P2	P11				
Glycolysis or Gluconeogenesis	P3					
Glyoxylate and dicarboxylate metabolism	P13					
Histidine metabolism	A1					

Inositol phosphate metabolism	P2					
Insect hormone biosynthesis	A1	P3				
Lysine biosynthesis	A1					
Lysine degradation	P2					
Metabolism of xenobiotics by cytochrome P450	A1	P2				
Nicotinate and nicotinamide metabolism	P2					
Pantothenate and CoA biosynthesis	A1	P18				
Pentose and glucuronate interconversions	A1	P18				
Pentose phosphate pathway	A1	L1	P1	P2	P3	P18
Phenylalanine metabolism	A1	P2				
Purine metabolism	L1	P1	P18			
Pyrimidine metabolism	A1	P11	study-wide			
Pyruvate metabolism	P13					
Starch and sucrose metabolism	A1	P3	P18			
Sulfur metabolism	P2					
Taurine and hypotaurine metabolism	L1	P1				
Tyrosine metabolism	P2	P3				
Ubiquinone and other terpenoid-quinone biosynthesis	P3					
Valine, leucine and isoleucine degradation	P18	study-wide				

Many metabolite features in our dataset were uniquely represented in manipulated samples: 454 features were never detected in healthy sham treatment ants and 1,781 additional features either were detected in less than 50% of the healthy ants and/or their median peak value was not at least double that of blank-collection controls (2,235 features total). These features may represent compounds tightly regulated and scarce in the healthy ant or uniquely produced by the fungus. We predicted that this feature set might have been enriched for hallmarks of infection and manipulation processes. However, no significant pathway enrichments were returned from our Mummichog and GSEA analyses. This could indicate that these metabolites are not linked by common metabolic pathways and/or many of these metabolites were not well annotated in the KEGG databases (e.g., species-specific metabolites).

We used a weighted gene co-expression network analysis (WGNCA) based approach to cluster metabolite features that similarly change abundance levels between healthy and manipulated *C. floridanus* treatments (Fig. 2C) (Langfelder and Horvath 2008). Co-expression (or co-abundance)

175 networks, in some cases, suggest linked biological functions and activity in the same metabolic processes
176 (Stuart *et al.* 2003; Carlson *et al.* 2006; Gillis and Pavlidis 2012; Bartzis *et al.* 2017). We detected three
177 biogenic amine, eight polyphenol, and five lipid network modules that were significantly correlated to
178 treatment (Fig. 4). A total of six biogenic amine (A1-A6), 19 polyphenol (P1-P19), and 10 lipid (L1-L10)
179 networks were created in total. Due to our sparse annotation

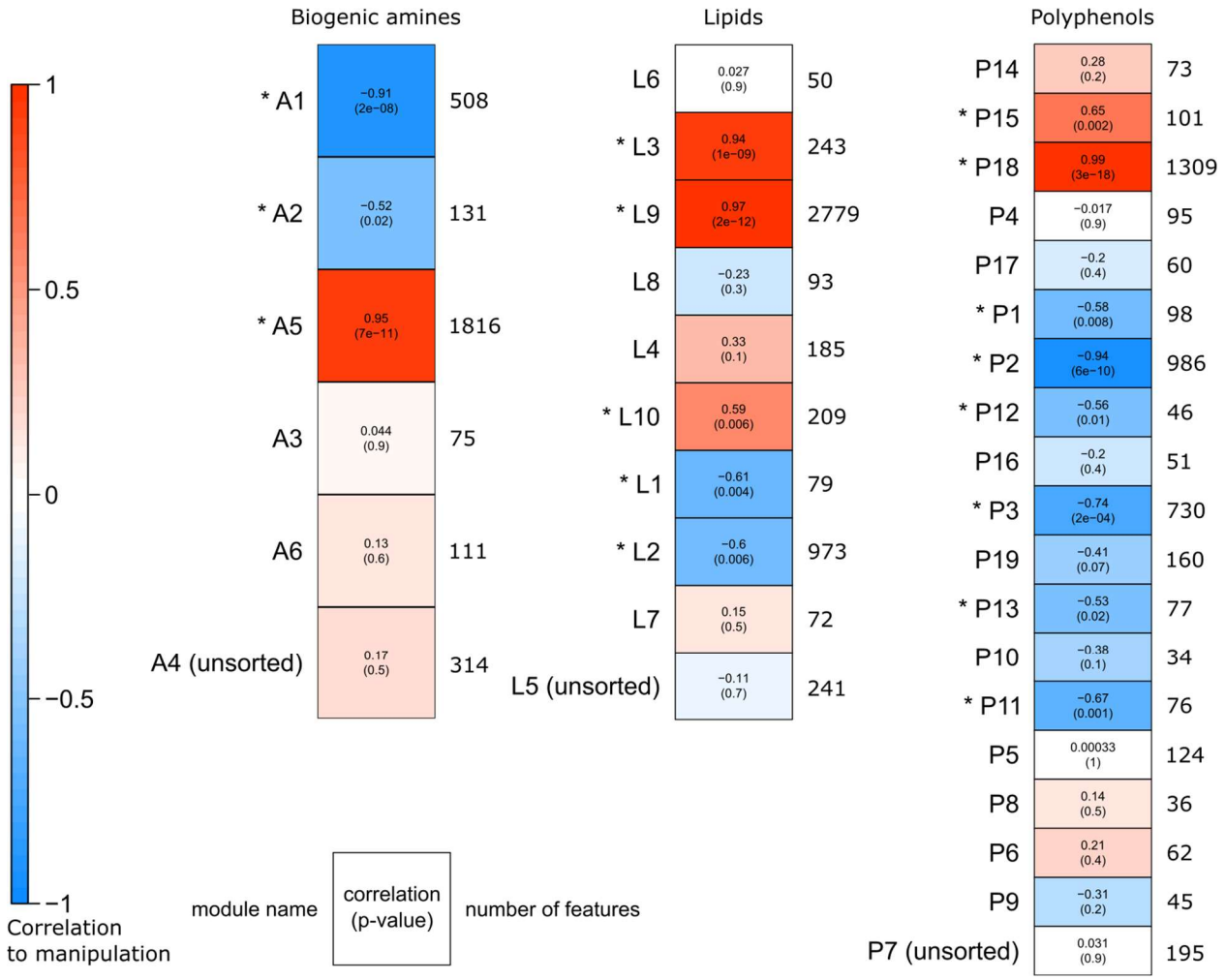

180

181 **Figure 4. WGCNA network modules of metabolite features and their correlation to manipulation.**
182 In total we detected three, five, and eight significantly correlated (Student correlation ≥ |0.5|, $p \leq 0.05$, denoted with
183 *) network modules to manipulation in the biogenic amines, lipids, and polyphenol datasets, respectively. Network
184 modules were constructed as unsigned, meaning the direction of the correlation describes the network as a whole,
185 although some features may be anti-correlated within the module. "Unsorted" modules contain all features that were
186 not successfully correlated to other features in a network (i.e., by default labeled "gray" by R package WGCNA).
187

188 data, we were not able to consistently compare hub features. As such, we considered all available
189 annotations within a network module and Mummichog pathway enrichments (Fig. 2C). Across all
190 network modules significantly correlated to the transition from healthy to manipulated ants, 44 unique
191 enriched KEGG pathways were selected, which included the eight found across the study-wide data that
192 passed at least two selection filters (Table 6, Supp. Data 2).

193 **The biogenic monoamine neurotransmitters dopamine, serotonin, and octopamine are**
194 **known to modulate ant activity and may be proximate drivers of diseased behaviors:** A combination
195 of pathway enrichments, annotated DAMs, and DEGs suggest that shifts in metabolism associated with
196 neurotransmitters relate to behavioral alterations in *C. floridanus* infected and manipulated by *O.*
197 *camponoti-floridani*. The monoamine neurotransmitters dopamine, serotonin, and octopamine (analogous
198 to vertebrate norepinephrine) have been implicated in modulating locomotor, foraging, learning, social,
199 reproductive, and aggressive behaviors in many insects, and have been tested in social insects, including
200 ants (Adamo 2008; Aonuma and Watanabe 2012; Adamo *et al.* 2013; Kamhi *et al.* 2017; Verlinden
201 2018). Serotonin, octopamine, and melanin derived from L-3,4-dihydroxyphenylalanine (L-DOPA), or
202 tyrosine and dopamine, have roles in insect immunity as well (Geun *et al.* 2009; González-Santoyo and
203 Córdoba-Aguilar 2012). Administration of dopamine and serotonin to *Formica polyctena* wood ants or
204 *Odontomachus kuroiwae* trap-jaw ants have produced altered behaviors in the laboratory, such as
205 aggressive mandible-opening or biting behaviors and defensive responses (Szczuka *et al.* 2013; Aonuma
206 2020). In the field, *Pogonomyrmex barbatus* harvester ant dopamine levels positively correlated with
207 foraging trips, as seen both by dopamine supplementation and inhibition (Friedman *et al.* 2018).
208 Similarly, pharmacological depletion of serotonin led to reduced and impaired trail-following foraging
209 behavior in *Pheidole dentata* ants (Muscedere *et al.* 2012). In *Formica aquilonia*, there is evidence for
210 octopamine increasing aggressive behaviors (Yakovlev 2018), however, clear signs of increased
211 aggression with octopamine treatment was not found in *F. polyctena* (Szczuka *et al.* 2013). Octopamine
212 additionally appears to modulate the social behavior of trophallaxis in *Camponotus fellah*, while serotonin
213 had no significant effect (Boulay *et al.* 2000). As such, the exact effects of these neurotransmitters can

214 differ by species and social or physiological context. However, many of these affected behaviors are
215 relatable to the disease phenotypes observed in *Ophicordyceps* infected ants. Observations of
216 *Ophiocordyceps*-infected ants include changes in behavior leading to increased walking, deviation from
217 foraging trails, reduced nestmate communication, and the final manipulated bite (Pontoppidan *et al.* 2009;
218 Andersen *et al.* 2009; Hughes *et al.* 2011; de Bekker *et al.* 2015; Trinh *et al.* 2021).

219 Furthermore, gene expression networks negatively correlated between the ant and fungus were
220 enriched for host neuronal function and parasite manipulation-associated secreted proteins. This
221 correlation suggested parasite effectors promote, directly or indirectly, the downregulation of host gene
222 modules related to neuronal maintenance, circadian rhythm, olfaction, and memory (Will *et al.* 2020).
223 Additionally, direct host-parasite interactions have been hypothesized to occur by fungal proteins binding
224 ant neuroreceptors for dopamine, serotonin, and octopamine (Will *et al.* 2022 preprint). Although we did
225 not directly identify dopamine, serotonin, or octopamine in our metabolomic data, we did measure
226 features annotated as biosynthetically related compounds.

227 *Changes in dopamine metabolism possibly modified ant behaviors and shifted host-pathogen*
228 *immunological interactions during manipulation.* A combination of metabolomic and transcriptomic data
229 indirectly suggest increased dopamine metabolism in manipulated ants. The metabolomic signals
230 consisted of changes in neurotransmitter precursor abundances and enrichment of pathways in metabolite
231 network modules correlated to manipulation. Phenylalanine and tyrosine are precursors in synthesis
232 pathways for dopamine and octopamine. KEGG pathway "phenylalanine metabolism" was enriched in
233 both network modules A1 and P2 ($p = 0.026$ and 0.028, fold-enrichment = 1.5 and 1.9, respectively), both
234 of which were negatively correlated to manipulated ant samples. Additionally, KEGG pathway "tyrosine
235 metabolism" was enriched in modules P2 and P3 ($p = 0.030$ and 0.024, fold-enrichment = 1.4 and 1.6,
236 respectively), both also negatively correlated to manipulation. Moreover, module P2 also contained the
237 most informative compound annotations regarding dopamine metabolism.

238 The immediate precursor to dopamine, L-DOPA, was 2.8-fold reduced in abundance in
239 manipulated ants ($p = 0.008$, and in the top-50% of PC1) (Fig. 5). L-tyrosine was also annotated in

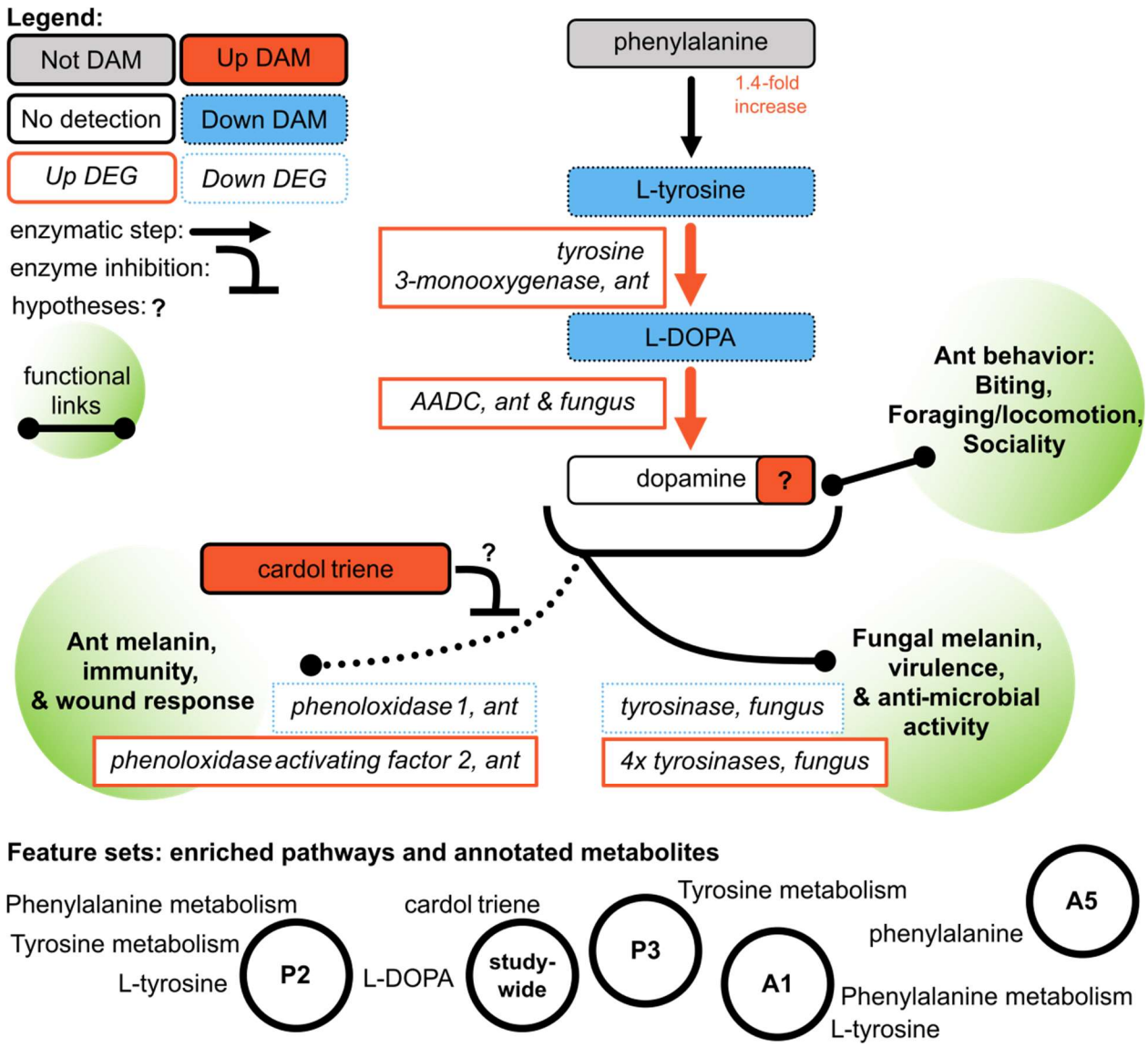

Figure 5. Altered neurotransmitter precursor metabolism suggests suppressed ant immunity, increased dopamine and serotonin, and reduced octopamine during infection and manipulation. Cardol triene may produced by the fungus to suppress ant immunity and thereby also increase availability of tyrosine and L-DOPA for dopamine synthesis. L-amino acid decarboxylase (AADC) catalyzes the final step of dopamine and serotonin synthesis and is upregulated by manipulated ants. A reduction of L-DOPA and tryptophan suggest that these compounds are being converted into dopamine and serotonin, respectively. Upregulation of an ant kynurenine aminotransferase possibly increases or maintains (if the kynurenine precursor is reduced) kynurenic acid levels. The possible of reduction of octopamine concentration follows the reasoning that it requires L-tyrosine for its synthesis, which is reduced during manipulation, and there is no compensatory upregulation of enzyme genes in the octopamine pathway to compete with upregulated dopamine biosynthesis. Dysregulated ant behavior during infection and manipulation may arise due to this altered neurotransmitter metabolism. Network modules from which

252 discussed feature annotations or enriched pathways reside are given at the bottom of the figure. Increases are
253 indicated by solid lines and red color, decreases by dotted lines and blue color, metabolites are in rounded
254 rectangles, genes are in rectangles, annotated metabolites that were not DAMs have gray color, compounds with
255 white color were not identified in the LC-MS/MS data, and hypothesized functional links are given in the shaded
256 circles. Metabolic steps that did not have DEG are shown as black arrows when useful for context but are omitted
257 elsewhere. A squiggled arrow indicates metabolite interaction with a receptor. Tryptophan is given colored as a
258 reduced abundance DAM, but was selected rather by the Boruta analysis only and not the differential abundance t-
259 test.
260
261 module P2 and is the precursor to L-DOPA and tyramine. The latter can be converted into the
262 neurotransmitter octopamine. L-Tyrosine was a DAM with a 2.1-fold decrease in abundance ($p = 1E-4$,
263 and Boruta confirmed). An annotation for tyrosine was also present in the network module A1, however,
264 we did not identify this metabolite feature as a DAM ($p = 0.154$, 1.2-fold reduction). Outside of network
265 modules A1, P2, and P3, we also detected phenylalanine, the precursor to tyrosine. Phenylalanine showed
266 a modest increase in abundance during manipulation just below our 1.5-fold change threshold for
267 classification as a DAM ($p = 0.019$, 1.4-fold increase) (Fig. 5). Decreases in L-tyrosine and L-DOPA
268 could be difficult to interpret alone, however in combination with RNAseq data, we found evidence for
269 increased dopamine synthesis that offers one explanation for the depletion of these dopamine precursors.
270 During manipulation, both ant hosts and fungal parasites upregulated an aromatic L-amino acid
271 decarboxylase (AADC) gene (Fig. 5). This enzyme catalyzes the final step of L-DOPA conversion to
272 dopamine and the conversion of L-5-hydroxytryptophan to serotonin (Dakshinamurti *et al.* 2017). The
273 AADC enzyme requires vitamin B6 as a cofactor and we detected differential abundance of an inactive
274 vitamer form and a precursor for *de novo* synthesis in module A5 (Supp. File 2). However, the
275 combination of metabolomic and transcriptomic data available do not provide for a clear interpretation for
276 if active vitamin B6 is changing in abundance and in which organism(s).
277 A tyrosine 3-monooxygenase, which catalyzes the rate-limiting conversion of L-tyrosine to L-
278 DOPA, was upregulated by manipulated ants. Meanwhile, the ant homolog to Henna (i.e., DTPHu
279 phenylalanine 4-monooxygenase), which converts phenylalanine to L-tyrosine was not differentially

280 expressed. This enzyme also converts peripheral tryptophan to the serotonin precursor in *D. melanogaster*
281 (Neckameyer and White 1992; Coleman and Neckameyer 2005; Neckameyer *et al.* 2007). This consistent
282 expression may help explain the only modest change of phenylalanine during manipulation while its
283 derivatives were found at lower concentrations.

284 Dopamine and its precursors can also be converted into melanin, a key compound for insect
285 wound response and immunity (González-Santoyo and Córdoba-Aguilar 2012; Sugumaran and Barek
286 2016; Wang *et al.* 2017). Fungi can also synthesize melanin for use in host-pathogen interactions and
287 against competing microbes (Nosanchuk and Casadevall 2006; Nosanchuk *et al.* 2015). We found
288 evidence that this pathway for melanin production is reduced in the ant during manipulation and,
289 possibly, increased in the fungus (Fig. 5).

290 We propose that the production of a fungal-derived compound may inhibit tyrosinases necessary
291 to convert dopamine-pathway metabolites to melanin and hence simultaneously steer these metabolites
292 toward dopamine production. This metabolite feature was annotated as cardol triene (i.e., 5-(8,11,14-
293 pentadecatrienyl)resorcinol) and was a DAM only detected in manipulated ant samples ($p = 0.0073$,
294 median peak value = 19,604, in the top 50% of PC1) (Fig. 5). As cardol triene was never detected in
295 healthy ants, it plausibly is produced solely by the fungus, although we cannot discount the possibility
296 that production of this metabolite is produced by ants combatting infection and completely absent in
297 healthy individuals. We detected the putative cardol triene in six of 10 manipulation samples, this could
298 indicate that cardol triene levels are tightly regulated. Cardol triene has been shown to inhibit tyrosinase
299 oxidation of L-DOPA (Zhuang *et al.* 2010). In insects, phenoloxidases are a type of tyrosinase and are
300 key enzymes that begin the conversion of dopamine and L-DOPA to pro-immune melanin production
301 pathways (Gorman and Arakane 2010; González-Santoyo and Córdoba-Aguilar 2012; Wang *et al.* 2017).
302 As such, we hypothesize that fungal cardol triene chemically inhibits host phenoloxidase activity to
303 reduce melanin metabolism.

304 Additionally, ants showed mixed transcriptional signals related to the melanin-immune response
305 by phenoloxidase and phenoloxidase activating factor genes (Fig. 5) (Piao *et al.* 2005). Entomopathogen

306 infections suppress phenoloxidase activity in mosquitoes and the inhibition of activation of pro-
307 phenoloxidase has been hypothesized as a mechanism of fungal interference with insect host immunity
308 (Feng *et al.* 2015; Ramirez *et al.* 2018). In addition to suppressing host melanin production, the fungus
309 may be converting L-DOPA or related compounds into fungal melanin precursors, as four upregulated
310 and one downregulated tyrosinases were found during manipulation (Fig. 5). Three of the upregulated
311 fungal tyrosinases are putatively secreted and may possibly interact with host tyrosine and its derivatives.
312 The sum result of this proposed altered dopamine metabolism could weaken host immunity, bolster
313 parasite pathogenicity, and drive altered host behavior by increased dopamine concentration (Fig. 5).
314 *Serotonin and octopamine metabolism may also correlate to manipulated ant behavior.*
315 Biosynthetically and phenotypically intertwined with dopamine, fluctuating serotonin and octopamine
316 concentrations may contribute to manipulated ant behavior. Although the metabolomic signals for these
317 compounds were less robust than for dopamine, we found multiomic evidence that offers support for
318 hypotheses of increasing serotonin and decreasing octopamine (Supp. File 3). For example, upregulation
319 of the AADC enzyme shared between dopamine and serotonin pathways and at least one signal for the
320 reduction of tryptophan (selected by Boruta), which can be converted into the precursor for serotonin.
321 Coupled with the increasing serotonin, we additionally propose a hypothesis for increased kynueric acid,
322 which is also tied to tryptophan and may act as a neuroprotectant for heavily diseased and manipulated
323 ants (Supp. File 3).
324 *Multiomic synthesis of transcriptomic and metabolomic data.* Our hypotheses link enzyme gene
325 transcription and metabolite precursor abundance to predict an increase of dopamine with a reduction in
326 host melanin and immunity. Using similar reasoning, but with less robust metabolomic support, we
327 consider increases of serotonin and kynurenic acid, while octopamine may be reduced (Supp. File 3). An
328 alternative interpretation of the data could be that increased gene expression does not indicate elevated,
329 functional protein abundance in every case, and may even be a homeostatic response to low enzyme
330 activity or substrate abundance. However, without new proteomic data, we suggest that inferring protein
331 levels by transcription to generally be the most parsimonious explanation. Similarly, reduced precursor

332 abundances could reflect wide-spread reduced levels of metabolites, including neurotransmitter products.
333 But in the context of the observed behavioral manipulation phenotypes and reconciling transcriptomic and
334 metabolomic data, we propose a set of hypotheses we deem most plausible. Regardless of whether each
335 neurotransmitter discussed is increased or decreased in abundance, our data link changes in
336 neuromodulatory processes and parasitically manipulated behavior.

337 **Altered glycerophospholipid metabolism suggested increased fungal cell membrane activity**
338 **and ant accumulation of the excitatory neurotransmitter, acetylcholine:** The KEGG pathway
339 "glycerophospholipid metabolism" was enriched in module P2 and in study-wide features passing at least
340 two selection filters (p =0.024 and 0.030, fold-enrichment = 1.9 and 1.4, respectively). We found
341 evidence for two possible major effects, changes in cell membrane composition and the accumulation of
342 acetylcholine. Of our annotated features, metabolic signals centered on choline offered the most insight
343 into altered glycerophospholipid metabolism. Glycerophospholipids and choline-containing compounds
344 have been associated with neurodegenerative disease, such as Alzheimer's or Parkinson's, and insect
345 host-pathogen responses (Walter *et al.* 2004; Hoxmeier *et al.* 2015; Alecu and Bennett 2019). Choline is a
346 key component involved in the synthesis of phospholipids associated with forming cell membranes,
347 especially as incorporated through phosphatidylcholine (Li and Vance 2008). Although, in fungi and
348 insects, phosphatidylethanolamine is also a major cell membrane component (Batrakov *et al.* 2001;
349 Dawaliby *et al.* 2016; Cassilly and Reynolds 2018). Using the lipids LC-MS/MS dataset we compared
350 peak values of phosphatidylethanolamines (n = 95 features) and phosphatidylcholines (n = 85 features)
351 and found phosphatidylethanolamines to indeed be abundant in our insect and fungal tissue samples.
352 Within healthy ants, phosphatidylethanolamines were only slightly more abundant (1.10-fold greater)
353 than phosphatidylcholines (t-test, p = 0.017, t = -2.657). Within fungus-manipulated ants, there was no
354 strong difference (t-test, p = 0.739, t = -0.339, phosphatidylethanolamines 1.05-fold higher). As both
355 phospholipid types were nearly equally abundant, we considered changes of metabolites of either class
356 could reflect important processes during manipulation.

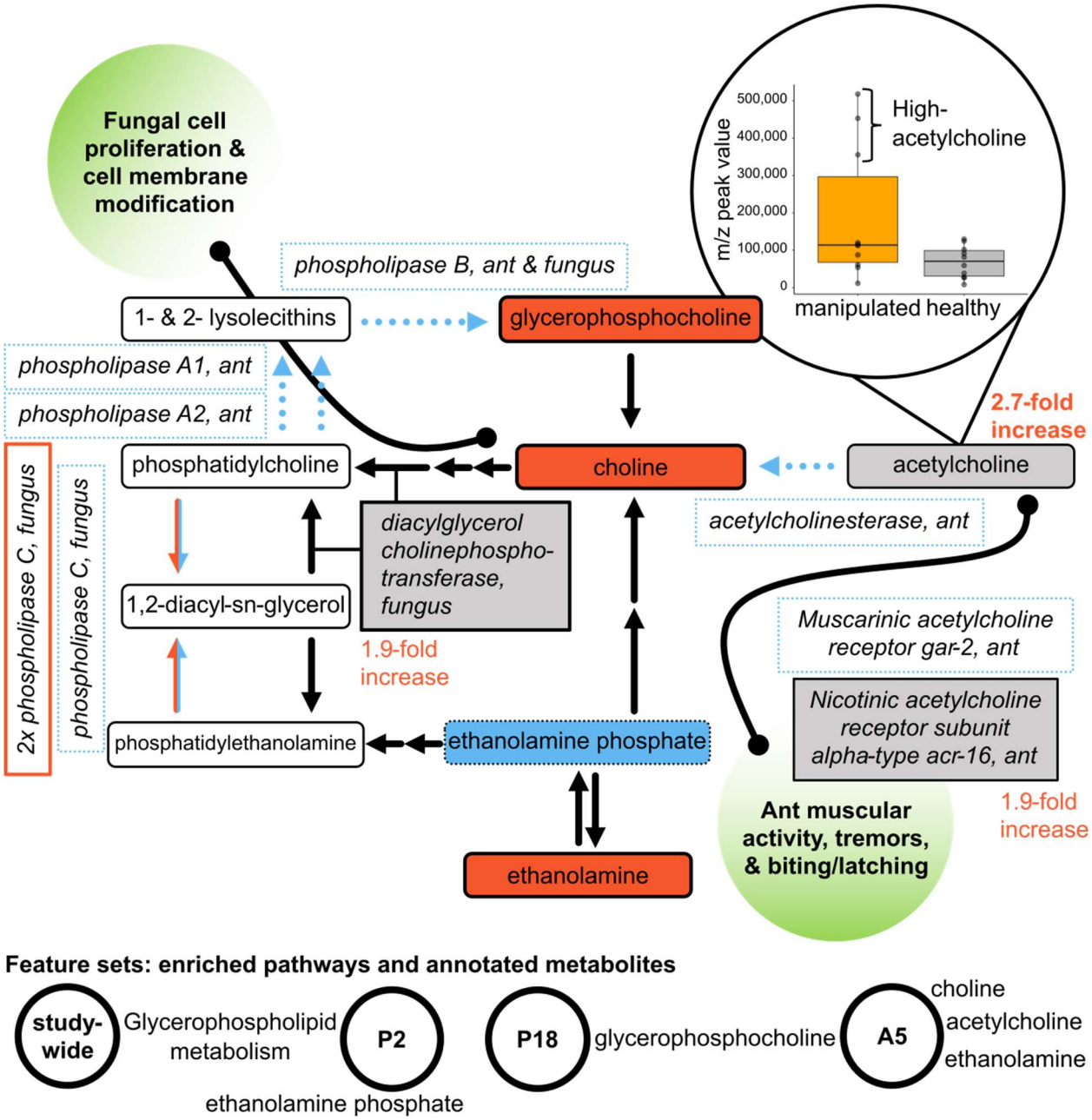

Figure 6. Changing glycerophospholipid metabolism during manipulation primarily indicate altered acetylcholine levels in the ant and cell membrane metabolism in the fungus.

Manipulated ant samples appeared to have two distinct groups, one with high acetylcholine and one with levels similar to healthy ants. In manipulated ants, the putative acetylcholinesterase and two acetylcholine receptor genes were downregulated, suggesting acetylcholine levels were accumulating. We hypothesize that increased acetylcholine in manipulated ants is associated with the increased muscular activity during early manipulation (e.g., tremors, biting, and latching behavior). Once the ant is secured in a summited position and the mandible muscles (and associated neurons) are further degraded, the fungus may be scavenging and converting the available acetylcholine to choline, thereby rapidly reducing acetylcholine levels. The fungus may be converting choline to

367 phospholipids, such as phosphatidylcholine to remodel and build cell membranes. Although we did detect multiple
368 features in the class of phosphatidylcholines and phosphatidylethanolamines, we did not identify the singular
369 metabolites "phosphatidylcholine" and "phosphatidylethanolamine" themselves. Network modules from which
370 discussed feature annotations or enriched pathways reside are given at the bottom of the figure. Increases are
371 indicated by solid lines and red color, decreases by dotted lines and blue color, metabolites are in rounded
372 rectangles, genes are in rectangles, annotated metabolites or genes that were not DAMs or DEGs have gray color,
373 compounds with white color were not identified in the LC-MS/MS data, and hypothesized functional links are given
374 in the shaded circles. Metabolic steps that did not have DEG are shown as black arrows when useful for context but
375 are omitted elsewhere. A squiggled arrow indicates metabolite interaction with a receptor.
376

377 Choline was a DAM increasing during manipulation (p = 1.7E-11, 20.0-fold increase, passing all
378 selection criteria) (Fig. 6). We also observed other DAMs related to choline within the
379 glycerophospholipid metabolism pathway. Glycerophosphocholine, a choline precursor was increased at
380 manipulation and detected in two datasets (p = 3.4E-11 and 1.2E-7, 5.9- and 7.7-fold increase, passing all
381 three selection criteria). We also detected two DAMs interconnected between choline and
382 phosphatidylethanolamine: ethanolamine (p = 5.2E-5, 2.1-fold increase, also Boruta confirmed) and
383 ethanolamine phosphate (p =1.6E-9, 5.5-fold decrease, passing all selection criteria) (Fig. 6). Three
384 putative *Ophiocordyceps* phospholipase C genes were DEGs, two upregulated and one downregulated
385 (Fig. 6). Broadly, phospholipid C proteins cleave phospholipids and have been implicated in cell
386 signaling, pathogenicity, and cell membrane metabolism (Pokotylo *et al.* 2013). When cleaving either
387 phosphatidylcholine or phosphatidylethanolamine they can produce an intermediate 1,2-diacyl-sn-
388 glycerol product. Additionally, the fungus expressed a putative diacylglycerol cholinephosphotransferase
389 gene 1.9-fold higher during manipulation, nearly qualifying as a DEG. This enzyme combines 1,2-diacyl-
390 sn-glycerol and CDP-choline to produce phosphatidylcholine. Phosphatidylcholine could then be
391 converted to glycerophosphocholine within two metabolic steps, but this pathway appeared to be
392 downregulated. Three genes putatively encoding the enzymes driving this conversion were downregulated
393 in the ant (phospholipases A1, A2, and B). In the fungus, a phospholipase B-like gene was also
394 downregulated (Fig. 6). The net effect appears to be fungal composition and/or catabolism of

395 phosphatidylethanolamines and synthesis of phosphatidylcholines leading to a minor compositional shift
396 overall during manipulation - but perhaps including specific and important changes we cannot yet identify
397 (Fig. 6). Modification of the cell membrane could be necessary to accommodate transmembrane proteins
398 or secretory activity involving organelle membranes such as in the endoplasmic reticulum (van der Veen
399 *et al.* 2017; Shyu *et al.* 2019).

400 Choline can also be metabolized into acetylcholine, the most abundant excitatory
401 neurotransmitter in insects (Gauthier 2010). In bees, excessive activation of acetylcholine receptors can
402 cause changes in locomotor, navigational, foraging, and social behaviors (Grünewald and Siefert 2019).
403 Acetylcholine can be rapidly converted back to choline by the activity of the acetylcholinesterase enzyme,
404 which has been a target of enzyme-inhibiting insecticides (Quinn 1987; Fournier *et al.* 1992; Colovic *et*
405 *al.* 2013; Singh *et al.* 2017). From this fast enzymatic activity, we intuit that acetylcholine levels could
406 reflect changes in physiology and behavior at a fine timescale. A subgroup of the manipulated ant
407 samples showed markedly higher acetylcholine levels than both healthy and other manipulated ants (Fig.
408 6). As such, we propose a scenario of transiently increased acetylcholine during manipulation, only
409 detected in a subset of our samples.

410 Acetylcholine showed a 2.7-fold mean increase at manipulation overall, but was not identified as
411 a DAM ($p = 0.142$), with a feature-peak value distribution showing two distinct groups. Three
412 manipulated ants had 5.5-fold higher acetylcholine peak values than the other seven that spanned a similar
413 range as control samples (Fig. 6). Speculatively, this could indicate that, for some fast-changing
414 metabolites such as acetylcholine, our sampling approach captured multiple subtly different physiological
415 states during the dynamic process of behavioral manipulation. The previously collected transcriptomics
416 data similarly showed the broadest distribution of acetylcholinesterase-2 expression during manipulation.
417 In the ant, an acetylcholinesterase-2-like gene was downregulated during active manipulation overall, but
418 two of the five samples had 2.5-fold lower acetylcholinesterase expression than the other three (Supp. Fig.
419 1) (Will *et al.* 2020). As the ant dies, acetylcholinesterase-2 expression begins to rebound toward healthy
420 ant levels. Notably, acetylcholinesterase-2 is the functionally dominant acetylcholinesterase enzyme in

421 *Camponotus* and many hymenopterans (Kim and Lee 2013). Additionally, the ant downregulated a
422 putative muscarinic acetylcholine receptor gar 2 that has been found in sensory and motor neurons of *C.*
423 *elegans* (Lee *et al.* 2000). Nearly a DEG as well, a putative ant nicotinic acetylcholine receptor acr-16
424 subunit gene was expressed 1.9-fold lower during manipulation. Possibly, receptor downregulation
425 represents a homeostatic response to the proposed elevated acetylcholine levels present during part of
426 manipulated summiting and biting.

427 Although acetylcholine has fast-acting regulatory effects on motor behavior, importantly,
428 glutamate is the direct primary excitatory neurotransmitter at insect neuromuscular junctions (Johansen *et*
429 *al.* 1989; Gauthier 2010; Pflüger and Duch 2011). Glutamate was nearly classified as a reduced DAM (p
430 = 0.007, 1.4-fold decrease) while a related compound, glutamine, did qualify (p = 1.8E-6 and 6.2E-11,
431 3.3- and 3.8-fold decrease, in network module A5 and also P2, respectively), with transcriptomic
432 evidence that suggested the host and parasite may be mounting contrasting regulatory responses (Will *et*
433 *al.* 2020) (Supp. File 4).

434 **Common metabolites between *Ophiocordyceps*-*Camponotus* manipulations in two species**
435 **pairings:** Previous metabolomic studies with *O. kimflemingiae* have identified many metabolites
436 associated with infection of *C. castaneus* and proposed links between these compounds and manipulation
437 (de Bekker *et al.* 2014b; Zheng *et al.* 2019; Loreto and Hughes 2019). Laboratory co-culture of *O.*
438 *kimflemingiae* with brains from *C. castaneus* and other ant species showed shared metabolites and distinct
439 compounds reflecting a combination of target host-specific fungal secretions and ant species profile (de
440 Bekker *et al.* 2014b). Other studies have compared *O. kimflemingiae* infections to that by a generalist
441 entomopathogenic fungus, again finding both overlap and differences in metabolomic profiles (Zheng *et*
442 *al.* 2019; Loreto and Hughes 2019).

443 Ergothioneine, an amino acid produced by some fungi, but not animals, has been detected in
444 mixed ant-fungal tissue from manipulated ant brains and muscles (Zheng *et al.* 2019; Loreto and Hughes
445 2019). Corroborating these findings, we detected two ergothioneine signals (biogenic amine and
446 polyphenol datasets) that were wholly absent in the healthy ants or with peak values near that of blank-

447 collection samples (p = 7.3E-15 and 4.6E-12, passing all selection criteria). In addition to fungal
448 metabolism, ergothioneine has been discussed as a possible neuroprotectant to preserve the ant brain until
449 manipulated summiting and biting are complete (Loreto and Hughes 2019). Supporting this line of
450 reasoning, ergothioneine in the ant brain was not detected at elevated levels in moribund ants infected by
451 the generalist entomopathogen *Cordyceps bassiana* that consumes hosts more quickly, without inducing
452 summit disease, and appears to occupy the ant head capsule to a lesser extent than *Ophiocordyceps*
453 (Fredericksen *et al.* 2017; Loreto and Hughes 2019).

454 Previous work with *O. kimflemingiae* and this work with *O. camponoti-floridani* have found
455 adenosine and adenosine-phosphate (AMP) to be differentially abundant between manipulation and
456 healthy and/or generalist-infected ants (Zheng *et al.* 2019; Loreto and Hughes 2019). We found two
457 features annotated as adenosine, one which was not differentially abundant and one that was a reduced
458 DAM in manipulated samples (p = 6.6E-4, 2.5-fold decrease). In contrast, previous works found
459 adenosine to increase in abundance in both manipulated ant brains and mandible muscles (Zheng *et al.*
460 2019; Loreto and Hughes 2019). Whether these contrasting results indicate species-specific patterns or
461 high variation is unclear. We also found decreased AMP (p = 0.003, 2.1-decrease, Boruta confirmed) in
462 the head, as was found in manipulated *C. castaneus* (Zheng *et al.* 2019; Loreto and Hughes 2019). In *O.*
463 *kimflemingiae* infection, a role for adenosine mediated neuromodulation was hypothesized, as was
464 changing AMP levels possibly reflecting changes in mitochondrial activity (Zheng *et al.* 2019; Loreto and
465 Hughes 2019). Cyclic AMP is involved in many pathways, including as a secondary messenger in G-
466 protein coupled receptor signaling, which includes receptors for dopamine and other neurotransmitters,
467 and have been hypothesized to be implicated in manipulation based on gene expression and host-parasite
468 protein-protein interaction predictions (Will *et al.* 2020, 2022 preprint). If changing abundance of AMP
469 reflects upon the cyclic form as well, this could relate to dysregulation of receptor signaling.
470 Metabolically related to adenosine, hypoxanthine and inosine were also proposed to have links to
471 energetic and neurological processes in manipulated ants (Zheng *et al.* 2019; Loreto and Hughes 2019).
472 As in those studies, we also detected increased levels of hypoxanthine during manipulation, two of three

473 features annotated as hypoxanthine increased at manipulation (p = 0.007 and 7.7E-6, 1.6-fold increase or
474 absent in sham, the latter of which passed all selection criteria). We also detected one inosine and two
475 inosine-monophosphate features increased in manipulated ants (p = 0.002, 3.8E-7, and 1.4E-5, 1.9-, 2.8-,
476 2.5-fold increase, all Boruta confirmed). This could indicate the conversion of AMP and adenosine to
477 hypoxanthine primarily via inosine intermediates.

478 **Pathways and compounds with reduced multiomic support:** Metabolomics results without
479 robust multiomic support or clearly annotated metabolite features provide a basis for future investigations.
480 Pathway enrichments without high-confidence metabolite annotations suggested possible changes in
481 insect hormone and detoxification metabolism during manipulation (Supp. File 5). With supporting
482 metabolite annotations but lacking strong genomic or transcriptomic evidence, we speculate that the
483 fungus may synthesize a cytoprotectant (carnosine), which could be derived from host compounds and
484 protect key host tissues (e.g., brain) during infection (Supp. File 5).

485

486 **Conclusion**

487 Infection and behavioral manipulation of hosts could involve many interacting molecular and
488 cellular processes. As these host-parasite interactions are better characterized, we can also gain insights
489 into specialist co-evolutions, the mechanistic basis of animal behavior, and the discovery of new bioactive
490 compounds. To unravel the mechanistic complexity of infection and manipulated host behavior, we
491 require functional tests built upon robust hypotheses. Towards this goal, we studied parasitic
492 manipulation of *C. floridanus* by *O. camponoti-floridani*, combining metabolomic, transcriptomic, and
493 genomic data to develop a set of hypotheses regarding molecular processes during manipulation.

494 We found evidence for altered biogenic monoamine neurotransmitter production during infection
495 and manipulation that may be proximate causes of manipulated behavior. In total, we propose a scenario
496 where the manipulated ant has elevated production of dopamine, with possible increases of serotonin and
497 decreases of octopamine. The fungus may also simultaneously suppress the host's melanin and immunity
498 pathways while metabolizing dopamine and its precursors for fungal melanin production. Ants infected

499 by *Ophiocordyceps* display enhanced locomotion/activity levels, reduction of social behaviors, and a final
500 summit latching behavior – elements of these behaviors have already been associated with
501 neurotransmitter signaling in ants. Intriguingly, aquatic gammarid crustaceans manipulated by
502 acanthocephalan worms display a phototactic summiting and clinging phenotype in the water column
503 sometimes associated with increased serotonin, decreased octopamine, and suppressed phenoloxidase-
504 mediated immunity – essentially, parts of the same pattern we propose in manipulated *Camponotus*
505 (Helluy and Holmes 1990; Lefèvre *et al.* 2009; Helluy 2013; Herbison 2017). Manipulators of vertebrate
506 behavior may also leverage serotoninergic and dopaminergic processes to alter fish and mouse behaviors
507 related to escape responses, locomotion, and aggression (Shaw *et al.* 2009; Prandovszky *et al.* 2011;
508 Adamo *et al.* 2013; Lafferty and Shaw 2013). How much of the alteration of neurotransmitter metabolism
509 may be a general response to fungal infection and how much results from specific manipulation by
510 *Ophiocordyceps* is difficult to pinpoint at this time. However, cardol triene appears to be a fungal derived
511 compound that could suppress ant immunity and increase substrate availability for dopamine production.
512 Also, *Ophiocordyceps* upregulated three putatively secreted tyrosinases that possibly interact with host
513 dopamine/melanin precursors. Although less typically reported than their intracellular counterparts,
514 extracellular fungal tyrosinases have also been found in another fungus (Selinheimo *et al.* 2006;
515 Gasparetti *et al.* 2012). Dopamine, serotonin, and octopamine receptors appear to be directly targeted by
516 secreted fungal effector proteins as well (Will *et al.* 2022 preprint). Given the importance this may place
517 on a functional host brain and body, indications in our data for altered neuro/cyto-protectant
518 concentrations and detoxification metabolism may indeed reflect key changes in the manipulated
519 metabolome. Although, further evidence is required to fully assess this.
520 Changing glycerophospholipid metabolism during manipulation, largely centered on choline,
521 suggested fungal biosynthesis of cell membrane components and dysregulation of acetylcholine levels in
522 the ant. *Ophiocordyceps* may require increased choline-derived cell-membrane components used during
523 cell proliferation and membrane remodeling for structures such as lipid rafts or transmembrane proteins
524 important during infection and manipulation. Manipulated ants reduced expression of

525 acetylcholinesterase, and three metabolomic manipulation samples had notably higher acetylcholine
526 concentrations than the rest. Speculatively, transient high acetylcholine could contribute to summiting and
527 wandering behavior (i.e., increased locomotion), tremors, and the hypercontracted biting that locks
528 manipulated ants into place.

529 By inducing changes in neurotransmitters that regulate behavior in healthy ants, the fungus may
530 be impinging upon existing host systems to modify behavior rather than forcibly introducing novel
531 pathways. Indeed, many of the hallmark phenotypes of infection by ant-manipulating *Ophiocordyceps* are
532 not so dissimilar from activities influenced by levels of dopamine, serotonin, octopamine, and
533 acetylcholine in eusocial insects: foraging/locomotor behavior (i.e., summiting and hyperactivity),
534 sociality (i.e., wandering and reduced communication), and the biting/aggression (the final "death grip"
535 bite). Changes in social behavior could not only be a symptom of disease, but contribute to it as well. As
536 socially isolated infected ants may less frequently exchange trophallactic fluid with nestmates, these
537 infected individuals would lose an important source of nutrition, communication, and hormones (Leboeuf
538 *et al.* 2016) that may alter their metabolome. How exactly the fungus dysregulates physiological pathways
539 that influence behavior (e.g., juvenile hormone metabolism) and to what degree some level of
540 dysregulation is typical in many diseases is still unclear. These hypotheses can be further investigated by
541 functional tests (e.g., gene knockouts or dosing ants with metabolites) and LC-MS/MS validations of key
542 compounds using chemical standards.

543

544 **Methods**

545 **Ant collection & husbandry:** We used a single laboratory-housed wild-caught colony of *C.*
546 *floridanus* to produce all samples. This colony was collected in March 2021 in the University of Central
547 Florida arboretum. This colony had several hundred individuals including minors, majors, and brood.
548 Based on methods in Will *et al.* 2020, we housed the colony in a plastic container within a climate-
549 controlled incubator (I36VL, Percival) cycling 12 h-12 h, light-dark, 28 C°-20 C°, 65% RH-80% RH
550 daily cycles. Climate conditions cycled in a ramping manner, with a 4 h ramp from lights-on to a 4 h hold

551 at peak day conditions to a 4 h ramp to lights-off (additional husbandry details in Supp. File 6).

552 **Fungal strain OJ2.1 collection, culture, and storage:** *O. camponoti-floridani* strain OJ2.1 was
553 used to infect all ants in this work. We isolated this fungal strain using mycelium extracted from the
554 abdomen of a fresh, manipulated *C. floridanus* cadaver. This cadaver was found in the Ocala National
555 Forest, FL (29° 13' 41.7" N, 81° 41' 44.9" W). The isolation procedure, short ribosomal subunit genetic
556 validation, and culturing followed the protocols detailed in Will *et al.* 2020. In preparation for
557 experimental infections, we grew fungal cells for 10 days in liquid shaking cultures with Grace's medium
558 (Gibco) supplemented to 2.5% fetal bovine serum (Gibco) ("GF" medium). We then filtered (two-layers
559 of 12-ply gauze, Curity) and adjusted the blastospore cells to a working concentration of approximately 3
560 x 10^6 cells/mL (optical density 660 nm = ca. 0.5) prior to injection.

561 We have not incorporated isolated *in vitro* fungal control samples as was done for transcriptomic
562 analysis in Will *et al.* 2020. Such samples would not likely have been effective and efficient to include
563 given the higher number of samples required for robust LC-MS/MS analysis, fungal metabolite
564 production can be highly reflective of culture conditions (VanderMolen *et al.* 2013), and, unlike
565 transcriptomic analyses, we would not be able to discern the origin of metabolites in mixed-organism
566 manipulated ant samples regardless. Instead, we used the transcriptomic data to propose links of altered
567 metabolite abundances during manipulation to either the host or parasite.

568 **Experimental infections of ants:** Ten days before infection, we separated ants from their colony
569 into boxes per treatment group. For the *Ophiocordyceps*-infection treatment, we gathered 41 ants and 10
570 additional caretaker ants with painted abdomens (Testors paint), which did not receive the treatment but
571 assisted the 41 injected ants with recovery. One day before infection treatments, we removed the sugar
572 and water from the ant box to reduce the amount of fluid in the ants and ease the injection procedure. Due
573 to a husbandry accident that led to widespread death of the initial sham-infection treatment ants, we
574 repeated the sham treatment two weeks after the *Ophiocordyceps* experimental treatment. Ants from the
575 same colony were used for the sham treatment (n = 30 with 8 painted caretakers) and were maintained in
576 the same incubator as all other ants.

577 Ants were either anesthetized by placing their plastic box on top of ice prior to injection, or
578 directly injected at room temperature. We injected each ant with 0.5 µL *Ophiocordyceps* blastospores
579 (infection, n = 41) or 0.5 µL of GF (sham, n = 30) as detailed in Will *et al.* 2020. We placed the treated
580 ants and their painted caretaker ants in plaster-lined boxes with biting structures (*Tillandsia usneoides* tied
581 to wooden sticks with twine) and returned them to the climate-controlled incubator.

582 **Observation and sample collection for LC-MS/MS:** After 3 dpi we removed dead ants. Then,
583 we began screening for manipulated ants and deaths twice per day, at zeitgeber-time (ZT)-0, the
584 beginning of subjective day, and ZT-6, the mid-point of subjective day. At 10 dpi, we removed the
585 painted caretaker ants as previous work has observed *C. floridanus* to destroy and interfere with
586 manipulated nestmates, presumably as a component of their social immunity and nest hygiene (Diez *et al.*
587 2014; Will *et al.* 2020; Trinh *et al.* 2021). Starting 15 dpi, we began more frequent opportunistic checks
588 as behavioral manipulations of *C. floridanus* had been observed starting 19 dpi in the laboratory (Will *et*
589 *al.* 2020). After discovering the first manipulation at 21 dpi, we made multiple daily checks beginning at
590 ZT-20 and ending at ZT-14 (on the next subjective day). Previous laboratory *O. camponoti-floridani*
591 manipulations synchronized to the ants' subjective pre-dawn hours and we selected our observation times
592 to improve the odds of collecting manipulations close to their beginning (Will *et al.* 2020). We screened
593 non-manipulated mortalities for fungal infection by crushing tissue from the dead ant in 50 µL of water,
594 briefly touchdown centrifuging, and examining 15 µL of the supernatant on a microscope. Notable levels
595 of fungal cells were always and only seen in the *Ophiocordyceps* treatment ants. We analyzed and plotted
596 survival data using the R packages survival and survminer in R (v 4.1) with R Studio (v. 2021.09.2)
597 (RStudio Team 2015; Therneau 2015; Kassambara *et al.* 2019; R Core Team 2021).

598 *LC-MS/MS samples.* We collected live manipulated ants displaying characteristic summiting
599 biting behavior for LC-MS/MS immediately upon discovery (n = 20) (Fig. 2A). We subsequently
600 collected dpi-matched sham ants at ZT-21.5, as this was the most common time at which manipulated
601 ants were collected (n = 20) (see Results and Discussion, Fig. 2A). Manipulated ants found after death
602 were recorded for survival statistics but not used in the LC-MS/MS analyses (n = 3). For manipulated ant

603 collection, we clipped the biting substrate just above and below the manipulated ant and submerged the
604 ant in liquid nitrogen briefly until frozen. The sample was then placed in a pre-chilled, sterile 2 mL
605 microcentrifuge tube (USA Scientific) kept in liquid nitrogen until long-term storage at -80 C°. We
606 collected sham ant samples in a similar manner, plucked from the experiment box with forceps.

607 We created three blank-collection samples at the beginning, middle, and end of manipulated ant
608 sampling, i.e., after the first, 10th, and 20th manipulated ants were found (n = 3) (Fig. 2A). We made
609 blank-collection samples by briefly touching the forceps to the floor of the sham treatment housing boxes,
610 submerging them in liquid nitrogen, and swirling them in a microcentrifuge tube. We cleaned all tools and
611 surfaces with 70% ethanol and deionized water before sampling and between sample types.

612 We later prepared collected samples for LC-MS/MS by isolating ant heads. Each frozen ant was
613 quickly processed on a plastic petri dish (USA Scientific) on a bed of dry ice. Using forceps, we removed
614 biting substrate from the ant's mandibles if needed, snapped the head off, and placed it in a new
615 microcentrifuge tube. Heads were paired together by collection date into 10 two-head pools per treatment,
616 but later separated for analysis (see below). For blank-collection samples, we dragged the forceps along
617 the petri dish and swirled the forceps inside the original collection tube. We cleaned the tools and petri
618 dish with 70% ethanol and deionized water between individuals and used a new petri dish between
619 sample types. All samples and tubes were kept constantly chilled on dry ice or in liquid nitrogen.

620 **LC-MS/MS processing of ant head samples**: All samples were sent on dry ice to the West
621 Coast Metabolomics Center (WCMC, University of California, Davis) for LC-MS/MS analysis. The
622 WCMC processed samples in three LC-MS/MS protocols broadly tailored toward different chemistries:
623 "biogenic amines," "polyphenols and flavonoids," and "complex lipids." From the 20 samples collected
624 per infection and sham treatments, the WCMC collected polyphenol data for 10 individual ant heads, one
625 from each two-head pool. They used the remaining ten heads per treatment for biphasic extractions, with
626 each individual head used for both biogenic amines and lipids (Fig. 2A). Blank-collection samples were
627 shared across the three LC-MS/MS chemistries. The WCMC produced quality-control (QC) pool samples
628 consisting of all samples used per protocol and additional blank-extraction controls (Fig. 2A). These

629 WCMC control samples were run at the beginning and every ten samples thereafter per protocol. All LC-
630 MS/MS protocols collected MS/MS data in a top-four data-dependent-acquisition (DDA) mode in both
631 electrospray ionization (ESI) positive and negative modes.

632 The WCMC processed samples for biogenic amines for use in hydrophilic interaction
633 chromatography (HILIC) with quadrapole time of flight (Q-TOF) mass spectrometry. Homogenized ant
634 head samples were extracted with a methanol and methyl-tert-butyl ether protocol (Matyash *et al.* 2008)
635 and the aqueous phase used for biogenic amines LC-MS/MS and the organic phase used for lipids (see
636 below). Extractions were mixed with internal standards for normalization according to WCMC protocols
637 to a final volume of 100 µL (Supp. Data 3). Further details are provided in Supp. File 7.

638 Samples for lipids were processed for use in charged surface hybrid (CSH) chromatography with
639 Q-TOF mass spectrometry. The organic phase per biphasic extraction (shared with biogenic amines, see
640 above) was taken for lipids LC-MS/MS and mixed with internal standards according to WCMC protocols
641 (Supp. Data 3) to a final resuspension volume of 110 µL. Further details are provided in Supp. File 7.

642 Samples for polyphenols were processed for use in pentafluorophenyl (PFP) chromatography
643 with QExactive HF (QE) mass spectrometry. Homogenized ant head samples were extracted in a similar
644 fashion as described above and resuspended in a final 100 µL volume with internal standards (Supp. Data
645 3). Further details are provided in Supp. File 7.

646 **Metabolomic data processing & feature filtering:** The WCMC performed initial processing
647 steps on all samples to produce metabolomic feature lists consisting of mass/charge ratio (*m/z*), retention
648 time (rt), and value of quantification ion peaks. They aligned raw data with MS-DIAL (v 4.7.0) (Tsugawa
649 *et al.* 2015), subtracted signals detected in the blank-extractions produced in the core facility, removed
650 duplicate signals and isotopes, normalized samples by internal standards, and assigned compound and
651 adduct annotations based on manual MS/MS matching in Massbank, Metlin, and NIST14 databases and,
652 for lipids, with LipidBlast (v 68) (Kind *et al.* 2013) (Fig. 2B). The resulting data consisted of several
653 thousand features per dataset: biogenic amines (5605 total with 141 annotated), polyphenols (6178 total
654 with 158 annotated), and lipids (7021 with 517 annotated) (Supp. Data 4).

655 We applied additional feature quality control and data reduction methods to create a final list of
656 metabolite features to investigate. Features that had greater than 50% missing values within both sham
657 and infection treatments were removed. Similarly, we removed features with both median peak values
658 (sham and infection) less than double that of median blank-collection peaks. Following removal based on
659 missingness and peak values, we removed features that we determined to have signals too variable for
660 robust analysis based on their coefficient of variation (CV%, or relative standard deviation) (Fig. 2B). For
661 the biogenic amines and lipid datasets that had successful QC pool data returned, we applied a CV%
662 maximum threshold to remove peaks that varied greatly due to technical variation between QC pool
663 injections. We selected the CV% threshold as the lowest (i.e., strictest) value between 30% and a dataset
664 specific value determined from the distribution of CV% values. We calculated this data-specific value as
665 the 75th-quartile + 1.5*interquartile-range (IQR), as is used to identify extreme values or outliers in data
666 distributions (e.g., boxplots). For the lipids, the 1.5*IQR method produced CV 25% as the cutoff,
667 removing 5.7% of features. For biogenic amines, the 1.5*IQR CV% was greater than 30%; therefore,
668 30% was used, removing 6.6% of features. The WCMC reported that all polyphenol QC pools failed on
669 acquisition. Therefore, we ranked each feature by its lowest CV% (i.e., from either CV%-sham or CV%-
670 manipulated) and removed the highest 6.1% of features. We selected this 6.1% value because it was the
671 mean of the CV% removal rates of the biogenic amine and lipid datasets. Although we cannot fully
672 discount biological variation in biogenic amine peak values within a treatment, by selecting the lowest
673 CV% per feature (whether from the sham or infection treatment), we sought to remove only features that
674 had high CV% regardless of treatment. After all these filtering steps, we continued with 3268 biogenic
675 amine features (58% of initially collected), 4878 polyphenol features (79% of initial), and 6305 lipid
676 features (90% of initial).
677 We further applied a putative adduct calling step to consolidate unannotated features that may
678 represent different adducts of the same compound. Per LC-MS/MS dataset, we divided features by
679 treatment and ESI mode, and processed each of these subsets with Binner (v 1.0.0) (Kachman *et al.* 2020)
680 (Fig. 2B). Briefly, Binner compares metabolite features "binned" by rt and calls putative adduct

681 relationships between these features based on a table of possible adducts, feature *m/z*, and correlation of
682 peak values across samples. Data were split by treatment to avoid possibly conflating signals for different
683 compounds found in only one of the treatments as adducts of each other. Data were natural log
684 transformed, no additional deisotoping step was preformed, the mass tolerance was set to 0.005 Da
685 (biogenic amines and lipids) or 0.003 Da (polyphenols), and default settings were used elsewhere. For
686 biogenic amines and polyphenols, we searched for adducts used in KACHMAN *et al.* 2020. For lipids, we
687 supplemented this adduct table with an additional adduct set publicly available online (Fiehn Lab 2020).
688 We then reunited data subsets to create feature lists that included all peaks that were labeled as primary
689 ions or remained unannotated in either treatment group. In effect, this step only removed peaks that were
690 determined to be putative adduct peaks in both treatments, resulting in the final processed datasets for
691 analysis of: 2955 biogenic amines (90% of QC filtered peaks remained), 4315 polyphenols (88% of QC
692 filtered peaks), and 4924 lipids (78% of QC filtered peaks) (Supp. Data 1).

693 **Metabolomic data analysis & feature selection:** To select a single set of study-wide features of
694 interest combined across all three datasets, we applied three statistical approaches (Fig. 2C). For features
695 with values equal to zero, we imputed zeros as 20% of the minimum value measured for that feature.
696 Each analysis we preformed was done independently per LC-MS/MS dataset (biogenic amines, lipids,
697 and polyphenols). We determined if a feature represented a DAM with a t-test (corrected FDR, $p \leq 0.05$)
698 and minimum ±1.5-fold change in abundance between sham and infection treatments. Principal
699 component analyses always indicated that only PC1 separated samples by treatment type (see Results). As
700 such, we noted features ranked in the upper 50% of PC1 absolute loading values. Given that our choice of
701 threshold was defined as half of the data, we did not rely on this test solely as merit for discussing a
702 feature, but rather as a way to add confidence to results of other analyses. Both t-tests and PCAs were
703 performed through the MetaboAnalyst interface (v 5.0) (Pang *et al.* 2021). Finally, we selected features
704 "confirmed" as "important" by Boruta (v 7.0.0, R package) random-forest based analyses with 900
705 maxRuns and 70,000 ntree settings (Kursa and Rudnicki 2010). In brief, "important" features are selected
706 by z-scores of mean decrease accuracy in decision trees in comparison to randomized versions of the data

707 (Kursa and Rudnicki 2010). Boruta offers an improvement over standard random-forest analyses for high
708 dimensional data such as in metabolomics, increasing the stability and robustness of the features selected
709 (Acharjee *et al.* 2020).

710 Additionally, we created co-abundance network modules of metabolite features per LC-MS/MS
711 dataset using the WGCNA method (Langfelder and Horvath 2008) (Fig. 2C). Although the WGCNA was
712 developed primarily for gene expression data, this technique has been used and evaluated for
713 metabolomic data as well (Bartzis *et al.* 2017). Heightened activity in a metabolic pathway could lead to
714 many compounds increasing. But simultaneously, their precursors may become depleted. Therefore,
715 correlations within a network could be both positive and negative. As such, we constructed unsigned
716 WGCNA modules. All WGCNA modules were constructed on feature data without imputing zeros, based
717 on the biweight midcorrelation to compare between treatment types (e.g., corFnc="bicor", robustY=F,
718 maxPOutlier=0.05) (R package WGCNA, v 1.67). In cases where zeros were present, the analysis
719 defaulted to the Pearson correlation for that feature. We obtained similar network modules when the
720 Pearson correlation was used for all features (data not shown). Soft power thresholds were selected
721 according to program recommendations as follows: biogenic amines – 3, polyphenols – 10, and lipids –
722 11.

723 We analyzed different groups of selected features for metabolic pathway enrichments. We formed
724 feature sets that combined data across all three LC-MS/MS datasets based on individual feature selection
725 analyses (t-test, PCA, and Boruta) or their presence only in manipulation samples. Dataset-specific
726 network modules were only analyzed with background features from the LC-MS/MS dataset they
727 belonged to and if the module was correlated to treatment (Student correlation $\geq |0.5|$, $p \leq 0.05$) (Fig. 2C).

728 We preformed Mummichog analyses on these feature sets (Li *et al.* 2013), as described in Results
729 & Discussion. This process matched 1,523 unique metabolite features to 6,725 KEGG annotated
730 compounds. For enrichment analyses combining features across datasets, we additionally used a
731 technique based on GSEA ranking features by t-scores returned by t-tests (Subramanian *et al.* 2005). In
732 network module pathway enrichment analyses, only Mummichog was used as it sets a hard threshold to

733 define a group of interest versus the background. Membership within or out of a network module was
734 simply defined and could be used for this division. All enrichment analyses were conducted through the
735 MetaboAnalyst interface with the following settings: Mixed ion mode, 3 ppm mass tolerance, retention
736 time included, primary ions not enforced, all adducts tested, default currency metabolites, and conducted
737 once for both the *Drosophila melanogaster* and *Saccharomyces cerevisiae* KEGG metabolic pathway and
738 compound databases (Fig. 2C). As we sought to characterize the composite metabolome of manipulated
739 ant heads containing both insect and fungal tissue, we chose both a well-studied insect and fungal model
740 organism to improve our odds of matching annotations. We did not use results from one database or the
741 other to discriminate between a host (ant) or parasite (fungus) signal. Neither of the databases would
742 represent the full metabolic repertoire of their respective model organisms and combining them could
743 offer more complete data for comparison. Furthermore, we wished to consider the possibility that due to
744 the relationship of the host and parasite, either organism may be producing metabolites canonically
745 associated with the other as part of its strategy in this antagonism.

746 We selected significantly enriched pathways based on one of the hypergeometric enrichment
747 results reported by MetaboAnalyst. When using Mummichog only (WGCNA module feature set), we
748 used the gamma-null adjusted p-value (≤ 0.05). When including a GSEA as a joint analysis (study-wide
749 feature set), we used the combined p-value (≤ 0.05), calculated with MetaboAnalyst using the Fisher
750 method. Of the overrepresented pathways selected by the enrichment analyses ($p \leq 0.05$), we further
751 imposed thresholds for: (*i*) a minimum of three selected features in the pathway, (*ii*) 1.25-fold enrichment,
752 and (*iii*) three DEGs (see below) encoding associated enzymes to discard weak signals that would likely
753 be difficult to interpret biologically in a multiomic pathway-level context (Fig. 2C). For cases when a
754 pathway was selected using both *D. melanogaster* and *S. cerevisiae* KEGG databases, a mean p-value and
755 fold-enrichment is reported.

756 **Multiomics integration of genomic and transcriptomic data:** We interpreted results of this
757 work's LC-MS/MS data in light of previously collected transcriptomic RNAseq data when possible (Will
758 *et al.* 2020). That RNAseq data was collected with a similar experimental framework, including

759 comparisons of gene expression of both *C. floridanus* and *O. camponoti-floridani* between a control
760 (uninfected ant or fungal culture) and manipulated ant samples. Identification of DEGs (Cuffdiff analysis
761 corrected FDR $p \leq 0.05$, minimum two-fold change, minimum 4 RPKM) and relevant statistics are
762 reported in Will *et al.* 2020. For each enriched metabolic pathway, we retrieved gene sequence data for
763 enzymes associated with that pathway in KEGG (by enzyme nomenclature EC number). For each enzyme
764 EC, we extracted the first representative gene listed for *D. melanogaster* and *S. cerevisiae*. We searched
765 for reciprocal best matches to those genes in both the *C. floridanus* and *O. camponoti-floridani* genomes
766 using Proteinortho (v 5) with default settings (Lechner *et al.* 2011). While this non-exhaustive approach
767 would not identify every possible *C. floridanus* or *O. camponoti-floridani* gene with homology to known
768 enzymes of interest, it did assist with initially selecting pathway enrichments for deeper analysis. Per
769 pathway, we required that at least three DEGs combined from both transcriptomes of the ant and fungus
770 had homologs to the enzymes associated with that pathway. This selection criterion followed the
771 pathway-level thinking to require at least three contributing metabolite features matched by Mummichog
772 to consider an enrichment result for discussion. Metabolic pathway relationships were based on KEGG
773 data and supplemented by other sources where cited.
774

775 **Data Availability**

776 Genomic and transcriptomic data referenced here are available in Will *et al.* 2020 and the
777 GenBank accessions reported therein. Supplemental Data files (Supp. Data 1-4) are available upon
778 request while at the preprint stage.
779

780 **Acknowledgments**

781 We would like to thank Sophia Vermeulen for assisting with testing fungal strain OJ2.1 and, with
782 Biplabendu Das, their help with ant infections and observations. We also thank Devin Burris for help with
783 ant monitoring. Jordan Dowell provided insightful discussions on LC-MS/MS methods and interpretation
784 for which we are grateful for. The Genetics Society of America provided travel support for dissemination

of early results of this work. Research funding for this project came from NSF (NSF-CAREER IOS-1941546 awarded to C.dB).

788 **References**

789 Acharjee, A., J. Larkman, Y. Xu, V. R. Cardoso, and G. V. Gkoutos, 2020 A random forest based
790 biomarker discovery and power analysis framework for diagnostics research. BMC Med. Genomics
791 13: 1–14.

792 Adamo, S. A., 2008 Norepinephrine and octopamine: linking stress and immune function across phyla.
793 ISJ 5: 12–19.

794 Adamo, S. A., 2019 Turning your victim into a collaborator: exploitation of insect behavioral control
795 systems by parasitic manipulators. Curr. Opin. Insect Sci. 33: 25–29.

796 Adamo, S. A., C. E. Linn, and N. E. Beckage, 2013 Parasites: evolution's neurobiologists. J. Exp. Biol.
797 216: 3–10.

798 Alecu, I., and S. A. L. Bennett, 2019 Dysregulated lipid metabolism and its role in α-synucleinopathy in
799 Parkinson's disease. Front. Neurosci. 13: 328.

800 Andersen, S. B., S. Gerritsma, K. M. Yusah, D. Mayntz, N. L. Hywel-Jones *et al.*, 2009 The Life of a
801 Dead Ant: The Expression of an Adaptive Extended Phenotype. Am. Nat. 174: 424–433.

802 Aonuma, H., 2020 Serotonergic control in initiating defensive responses to unexpected tactile stimuli in
803 the trap-jaw ant Odontomachus kuroiwae. J. Exp. Biol. 223:.

804 Aonuma, H., and T. Watanabe, 2012 Changes in the content of brain biogenic amine associated with early
805 colony establishment in the Queen of the ant, Formica japonica. PLoS One 7: e43377–e43377.

806 Bartzis, G., J. Deelen, J. Maia, W. Ligterink, H. W. M. Hilhorst *et al.*, 2017 Estimation of metabolite
807 networks with regard to a specific covariable: applications to plant and human data. Metabolomics
808 13: 129.

809 Batrakov, S. G., I. V. Konova, V. I. Sheichenko, S. E. Esipov, and L. A. Galanina, 2001 Two unusual
810 glycerophospholipids from a filamentous fungus, Absidia corymbifera. Biochim. Biophys. Acta -
811 Mol. Cell Biol. Lipids 1531: 169–177.

812 de Bekker, C., 2019 Ophiocordyceps–ant interactions as an integrative model to understand the molecular
813 basis of parasitic behavioral manipulation. Curr. Opin. Insect Sci. 33: 19–24.

814 de Bekker, C., W. C. Beckerson, and C. Elya, 2021 Mechanisms behind the Madness: How Do Zombie-
815 Making Fungal Entomopathogens Affect Host Behavior To Increase Transmission? (D. A. Garsin,
816 Ed.). MBio.
817 de Bekker, C., and B. Das, 2022 Hijacking time: How Ophiocordyceps fungi could be using ant host
818 clocks to manipulate behavior. Parasite Immunol. 44: e12909.
819 de Bekker, C., M. Merrow, and D. P. Hughes, 2014a From behavior to mechanisms: An integrative
820 approach to the manipulation by a parasitic fungus (Ophiocordyceps unilateralis s.l.) of its host ants
821 (Camponotus spp.). Integr. Comp. Biol. 52: 166–176.
822 de Bekker, C., R. A. Ohm, R. G. Loreto, A. Sebastian, I. Albert *et al.*, 2015 Gene expression during
823 zombie ant biting behavior reflects the complexity underlying fungal parasitic behavioral
824 manipulation. BMC Genomics 16: 620.
825 de Bekker, C., L. E. Quevillon, P. B. Smith, K. R. Fleming, D. Ghosh *et al.*, 2014b Species-specific Ant
826 Brain Manipulation by a Specialized Fungal Parasite. BMC Evol. Biol. 14: 166.
827 Boulay, R., V. Soroker, E. J. Godzinska, A. Hefetz, and A. Lenoir, 2000 Octopamine reverses the
828 isolation-induced increase introphallaxis in the carpenter ant Camponotus Fellah. Journgal Exp.
829 Biol. 203: 513–520.
830 Carlson, M. R. J., B. Zhang, Z. Fang, P. S. Mischel, S. Horvath *et al.*, 2006 Gene connectivity, function,
831 and sequence conservation: Predictions from modular yeast co-expression networks. BMC
832 Genomics 7: 1–15.
833 Cassilly, C. D., and T. B. Reynolds, 2018 PS, It's Complicated: The Roles of Phosphatidylserine and
834 Phosphatidylethanolamine in the Pathogenesis of Candida albicans and Other Microbial Pathogens.
835 J. Fungi 4:.
836 Coleman, C. M., and W. S. Neckameyer, 2005 Serotonin synthesis by two distinct enzymes in Drosophila
837 melanogaster. Arch. Insect Biochem. Physiol. 59: 12–31.
838 Colovic, M. B., D. Z. Krstic, T. D. Lazarevic-Pasti, A. M. Bondzic, and V. M. Vasic, 2013
839 Acetylcholinesterase Inhibitors: Pharmacology and Toxicology. Curr. Neuropharmacol. 11: 315.

840 Dakshinamurti, K., S. Dakshinamurti, M. P. Czubryt, K. Dakshinamurti, S. Dakshinamurti *et al.*, 2017
841 Vitamin B6: Effects of Deficiency, and Metabolic and Therapeutic Functions. Handb. Famine,
842 Starvation, Nutr. Deprivation 1–23.
843 Dawaliby, R., C. Trubbia, C. Delporte, C. Noyon, J. M. Ruysschaert *et al.*, 2016
844 Phosphatidylethanolamine Is a Key Regulator of Membrane Fluidity in Eukaryotic Cells. J. Biol.
845 Chem. 291: 3658.
846 Diez, L., P. Lejeune, and C. Detrain, 2014 Keep the nest clean: survival advantages of corpse removal in
847 ants. Biol. Lett. 10:.
848 Feng, P., Y. Shang, K. Cen, and C. Wang, 2015 Fungal biosynthesis of the bibenzoquinone oosporein to
849 evade insect immunity. Proc. Natl. Acad. Sci. U. S. A. 112: 11365–11370.
850 Fiehn Lab, 2020 ESI-MS-adducts-2020.
851 Fournier, D., J.-M. Bride, F. Hoffmann, and F. Karch, 1992 Acetylcholinesterase TWO TYPES OF
852 MODIFICATIONS CONFER RESISTANCE TO INSECTICIDE. J. Biol. Chem. 267: 14270–
853 14274.
854 Fredericksen, M. A., Y. Zhang, M. L. Hazen, R. G. Loreto, C. A. Mangold *et al.*, 2017 Three-dimensional
855 visualization and a deep-learning model reveal complex fungal parasite networks in behaviorally
856 manipulated ants. Proc. Natl. Acad. Sci. 114: 201711673.
857 Friedman, D. A., A. Pilko, D. Skowronska-Krawczyk, K. Krasinska, J. W. Parker *et al.*, 2018 The Role of
858 Dopamine in the Collective Regulation of Foraging in Harvester Ants. iScience 8: 283.
859 Gasparetti, C., E. Nordlund, J. Jänis, J. Buchert, and K. Kruus, 2012 Extracellular tyrosinase from the
860 fungus Trichoderma reesei shows product inhibition and different inhibition mechanism from the
861 intracellular tyrosinase from Agaricus bisporus. Biochim. Biophys. Acta - Proteins Proteomics
862 1824: 598–607.
863 Gauthier, M., 2010 *Insect Nicotinic Acetylcholine Receptors: State of the Art on Insect Nicotinic*
864 *Acetylcholine Receptor Function in Learning and Memory* (S. Hervé Thany, Ed.).
865 Geun, S. K., M. Nalini, Y. Kim, and D. W. Lee, 2009 Octopamine and 5-hydroxytryptamine mediate

866 hemocytic phagocytosis and nodule formation via eicosanoids in the beet armyworm, Spodoptera
867 exigua. Arch. Insect Biochem. Physiol. 70: 162–176.
868 Gillis, J., and P. Pavlidis, 2012 “Guilt by Association” Is the Exception Rather Than the Rule in Gene
869 Networks. PLOS Comput. Biol. 8: e1002444.
870 González-Santoyo, I., and A. Córdoba-Aguilar, 2012 Phenoloxidase: a key component of the insect
871 immune system. Entomol. Exp. Appl. 142: 1–16.
872 Gorman, M. J., and Y. Arakane, 2010 Tyrosine hydroxylase is required for cuticle sclerotization and
873 pigmentation in Tribolium castaneum. Insect Biochem. Mol. Biol. 40: 267–273.
874 Grünewald, B., and P. Siefert, 2019 Acetylcholine and Its Receptors in Honeybees: Involvement in
875 Development and Impairments by Neonicotinoids. Insects 10:.
876 Heil, M., 2016 Host Manipulation by Parasites: Cases, Patterns, and Remaining Doubts. Front. Ecol.
877 Evol. 4: 80.
878 Helluy, S., 2013 Parasite-induced alterations of sensorimotor pathways in gammarids: collateral damage
879 of neuroinflammation? J. Exp. Biol. 216: 67–77.
880 Helluy, S., and J. C. Holmes, 1990 Serotonin, octopamine, and the clinging behavior induced by the
881 parasite Polymorphus paradoxus (Acanthocephala) in Gammarus lacustris (Crustacea). Can. J. Zool.
882 68: 1214–1220.
883 Herbison, R. E. H., 2017 Lessons in Mind Control: Trends in Research on the Molecular Mechanisms
884 behind Parasite-Host Behavioral Manipulation. Front. Ecol. Evol. 5: 102.
885 Hoxmeier, J. C., B. D. Thompson, C. D. Broeckling, P. Small, B. D. Foy *et al.*, 2015 Analysis of the
886 metabolome of Anopheles gambiae mosquito after exposure to Mycobacterium ulcerans. Sci.
887 Reports 2015 51 5: 1–8.
888 Hughes, D. P., S. B. Andersen, N. L. Hywel-Jones, W. Himaman, J. Billen *et al.*, 2011 Behavioral
889 mechanisms and morphological symptoms of zombie ants dying from fungal infection. BMC Ecol.
890 11: 13.
891 Johansen, J., M. E. Halpern, K. M. Johansen, and H. Keshishian, 1989 Stereotypic morphology of

892 glutamatergic synapses on identified muscle cells of Drosophila larvae. J. Neurosci. 9: 710.
893 Kachman, M., H. Habra, W. Duren, J. Wigginton, P. Sajjakulnukit *et al.*, 2020 Deep annotation of
894 untargeted LC-MS metabolomics data with Binner. Bioinformatics 36: 1801–1806.
895 Kamhi, J. F., S. Arganda, C. S. Moreau, and J. F. A. Traniello, 2017 Origins of aminergic regulation of
896 behavior in complex insect social systems. Front. Syst. Neurosci. 11: 74.
897 Kanehisa, M., and S. Goto, 2000 KEGG: Kyoto Encyclopedia of Genes and Genomes. Nucleic Acids
898 Res. 28: 27.
899 Kassambara, A., M. Kosinski, P. Biecek, and S. Fabian, 2019 Drawing Survival Curves using "ggplot2"
900 [R package survminer version 0.4.4].
901 Kim, Y. H., and S. H. Lee, 2013 Which acetylcholinesterase functions as the main catalytic enzyme in the
902 Class Insecta? Insect Biochem. Mol. Biol. 43: 47–53.
903 Kind, T., K. H. Liu, D. Y. Lee, B. Defelice, J. K. Meissen *et al.*, 2013 LipidBlast in silico tandem mass
904 spectrometry database for lipid identification. Nat. Methods 2013 108 10: 755–758.
905 Kobmoo, N., D. Wichadakul, N. Arnamnart, R. C. Rodríguez De La Vega, J.-J. J. Luangsa-ard *et al.*,
906 2018 A genome scan of diversifying selection in Ophiocordyceps zombie-ant fungi suggests a role
907 for enterotoxins in co-evolution and host specificity. Mol. Ecol. 27: 3582–3598.
908 Kursa, M. B., and W. R. Rudnicki, 2010 Feature Selection with the Boruta Package. J. Stat. Softw. 36: 1–
909 13.
910 Lafferty, K. D., and J. C. Shaw, 2013 Comparing mechanisms of host manipulation across host and
911 parasite taxa. J. Exp. Biol. 216: 56–66.
912 Langfelder, P., and S. Horvath, 2008 WGCNA: an R package for weighted correlation network analysis.
913 BMC Bioinformatics 9: 559.
914 Leboeuf, A. C., P. Waridel, C. S. Brent, A. N. Gonçalves, L. Menin *et al.*, 2016 Oral transfer of chemical
915 cues, growth proteins and hormones in social insects. Elife 5:.
916 Lechner, M., S. Findeiß, L. Steiner, M. Marz, P. F. Stadler *et al.*, 2011 Proteinortho: Detection of (Co-
917)orthologs in large-scale analysis. BMC Bioinformatics 12: 1–9.

918 Lee, Y. S., Y. S. Park, S. Nam, S. J. Suh, J. Lee *et al.*, 2000 Characterization of GAR-2, a Novel G
919 Protein-Linked Acetylcholine Receptor from Caenorhabditis elegans. J. Neurochem. 75: 1800–1809.
920 Lefèvre, T., S. A. Adamo, D. G. Biron, D. Missé, D. Hughes *et al.*, 2009 Invasion of the body snatchers:
921 the diversity and evolution of manipulative strategies in host-parasite interactions. Adv. Parasitol.
922 68: 45–83.
923 Li, S., Y. Park, S. Duraisingham, F. H. Strobel, N. Khan *et al.*, 2013 Predicting Network Activity from
924 High Throughput Metabolomics. PLOS Comput. Biol. 9: e1003123.
925 Li, Z., and D. E. Vance, 2008 Thematic Review Series: Glycerolipids. Phosphatidylcholine and choline
926 homeostasis. J. Lipid Res. 49: 1187–1194.
927 Libersat, F., M. Kaiser, and S. Emanuel, 2018 Mind Control: How Parasites Manipulate Cognitive
928 Functions in Their Insect Hosts. Front. Psychol. 9: 572.
929 Loreto, R. G., and D. P. Hughes, 2019 The metabolic alteration and apparent preservation of the zombie
930 ant brain. J. Insect Physiol. 118: 103918.
931 Lovett, B., R. J. St. Leger, and H. H. de Fine Licht, 2020 Going gentle into that pathogen-induced
932 goodnight. J. Invertebr. Pathol. 174: 107398.
933 Mangold, C. A., M. J. Ishler, R. G. Loreto, M. L. Hazen, and D. P. Hughes, 2019 Zombie ant death grip
934 due to hypercontracted mandibular muscles. J. Exp. Biol. 222: jeb200683.
935 Matyash, V., G. Liebisch, T. V. Kurzchalia, A. Shevchenko, and D. Schwudke, 2008 Lipid extraction by
936 methyl-tert-butyl ether for high-throughput lipidomics. J. Lipid Res. 49: 1137–1146.
937 Moore, J., 2013 An overview of parasite-induced behavioral alterations - and some lessons from bats. J.
938 Exp. Biol. 216: 11–7.
939 Muscedere, M. L., N. Johnson, B. C. Gillis, J. F. Kamhi, and J. F. A. Traniello, 2012 Serotonin modulates
940 worker responsiveness to trail pheromone in the ant Pheidole dentata. J. Comp. Physiol. A
941 Neuroethol. Sensory, Neural, Behav. Physiol. 198: 219–227.
942 Neckameyer, W. S., C. M. Coleman, S. Eadie, and S. F. Goodwin, 2007 Compartmentalization of
943 neuronal and peripheral serotonin synthesis in Drosophila melanogaster. Genes, Brain Behav. 6:

944 756–769.
945 Neckameyer, W. S., and K. White, 1992 A single locus encodes both phenylalanine hydroxylase and
946 tryptophan hydroxylase activities in Drosophila. J. Biol. Chem. 267: 4199–4206.
947 Nosanchuk, J. D., and A. Casadevall, 2006 Impact of melanin on microbial virulence and clinical
948 resistance to antimicrobial compounds. Antimicrob. Agents Chemother. 50: 3519–3528.
949 Nosanchuk, J. D., R. E. Stark, and A. Casadevall, 2015 Fungal melanin: What do we know about
950 structure? Front. Microbiol. 6: 1463.
951 Pang, Z., J. Chong, G. Zhou, D. A. De Lima Morais, L. Chang *et al.*, 2021 MetaboAnalyst 5.0: narrowing
952 the gap between raw spectra and functional insights. Nucleic Acids Res. 49: W388–W396.
953 Pflüger, H. J., and C. Duch, 2011 Dynamic neural control of insect muscle metabolism related to motor
954 behavior. Physiology 26: 293–303.
955 Piao, S., Y. L. Song, H. K. Jung, Y. P. Sam, W. P. Ji *et al.*, 2005 Crystal structure of a clip-domain serine
956 protease and functional roles of the clip domains. EMBO J. 24: 4404.
957 Pokotylo, I., P. Pejchar, M. Potocký, D. Kocourková, Z. Krčková *et al.*, 2013 The plant non-specific
958 phospholipase C gene family. Novel competitors in lipid signalling. Prog. Lipid Res. 52: 62–79.
959 Pontoppidan, M. B., W. Himaman, N. L. Hywel-Jones, J. J. Boomsma, and D. P. Hughes, 2009
960 Graveyards on the move: The spatio-temporal distribution of dead ophiocordyceps-infected ants (A.
961 Dornhaus, Ed.). PLoS One 4: e4835.
962 Prandovszky, E., E. Gaskell, H. Martin, J. P. Dubey, J. P. Webster *et al.*, 2011 The Neurotropic Parasite
963 Toxoplasma Gondii Increases Dopamine Metabolism. PLoS One 6: e23866.
964 Quinn, D. M., 1987 Acetylcholinesterase: Enzyme Structure, Reaction Dynamics, and Virtual Transition
965 States. Chem. Reiviews 87: 955–979.
966 R Core Team, 2021 R: A language and environment for statistical computing.
967 Ramirez, J. L., E. J. Muturi, C. Dunlap, and A. P. Rooney, 2018 Strain-specific pathogenicity and
968 subversion of phenoloxidase activity in the mosquito Aedes aegypti by members of the fungal
969 entomopathogenic genus Isaria. Sci. Reports 2018 81 8: 1–12.

970 RStudio Team, 2015 RStudio: Integrated Development for R.

971 Sakolrak, B., R. Blatrix, U. Sangwanit, and N. Kobmoo, 2018 Experimental infection of the ant
972 Polyrhachis furcata with Ophiocordyceps reveals specificity of behavioural manipulation. Fungal
973 Ecol. 33: 122–124.

974 Selinheimo, E., M. Saloheimo, E. Ahola, A. Westerholm-Parvinen, N. Kalkkinen *et al.*, 2006 Production
975 and characterization of a secreted, C-terminally processed tyrosinase from the filamentous fungus
976 Trichoderma reesei. FEBS J. 273: 4322–4335.

977 Shaw, J. C., W. J. Korzan, R. E. Carpenter, A. M. Kuris, K. D. Lafferty *et al.*, 2009 Parasite manipulation
978 of brain monoamines in California killifish (Fundulus parvipinnis) by the trematode Euhaplorchis
979 californiensis. Proc. R. Soc. B Biol. Sci. 276: 1137–1146.

980 Shyu, P., B. S. H. Ng, N. Ho, R. Chaw, Y. L. Seah *et al.*, 2019 Membrane phospholipid alteration causes
981 chronic ER stress through early degradation of homeostatic ER-resident proteins. Sci. Reports 2019
982 91 9: 1–15.

983 Singh, K. D., R. K. Labala, T. B. Devi, N. I. Singh, H. D. Chanu *et al.*, 2017 Biochemical efficacy,
984 molecular docking and inhibitory effect of 2, 3-dimethylmaleic anhydride on insect
985 acetylcholinesterase. Sci. Reports 2017 71 7: 1–11.

986 Stuart, J. M., E. Segal, D. Koller, and S. K. Kim, 2003 A gene-coexpression network for global discovery
987 of conserved genetic modules. Science (80-.). 302: 249–255.

988 Subramanian, A., P. Tamayo, V. K. Mootha, S. Mukherjee, B. L. Ebert *et al.*, 2005 Gene set enrichment
989 analysis: A knowledge-based approach for interpreting genome-wide expression profiles. Proc. Natl.
990 Acad. Sci. U. S. A. 102: 15545–15550.

991 Sugumaran, M., and H. Barek, 2016 Critical Analysis of the Melanogenic Pathway in Insects and Higher
992 Animals. Int. J. Mol. Sci. 17:.

993 Szczuka, A., J. Korczyńska, A. Wnuk, B. Symonowicz, A. Gonzalez Szwacka *et al.*, 2013 The effects of
994 serotonin, dopamine, octopamine and tyramine on behavior of workers of the ant Formica polyctena
995 during dyadic aggression tests. Acta Neurobiol. Exp. (Wars). 73: 495–520.

996 Therneau, T., 2015 A Package for Survival Analysis in S.

997 Thomas, F., R. Poulin, and J. Brodeur, 2010 Host manipulation by parasites: A multidimensional
998 phenomenon. Oikos 119: 1217–1223.

999 Trinh, T., R. Ouellette, and C. de Bekker, 2021 Getting lost: the fungal hijacking of ant foraging
1000 behaviour in space and time. Anim. Behav. 181: 165–184.

1001 Tsugawa, H., T. Cajka, T. Kind, Y. Ma, B. Higgins *et al.*, 2015 MS-DIAL: data-independent MS/MS
1002 deconvolution for comprehensive metabolome analysis. Nat. Methods 2015 126 12: 523–526.

1003 VanderMolen, K. M., H. A. Raja, T. El-Elimat, and N. H. Oberlies, 2013 Evaluation of culture media for
1004 the production of secondary metabolites in a natural products screening program. AMB Express 3:
1005 71.

1006 van der Veen, J. N., J. P. Kennelly, S. Wan, J. E. Vance, D. E. Vance *et al.*, 2017 The critical role of
1007 phosphatidylcholine and phosphatidylethanolamine metabolism in health and disease. Biochim.
1008 Biophys. Acta - Biomembr. 1859: 1558–1572.

1009 Verlinden, H., 2018 Dopamine signalling in locusts and other insects. Insect Biochem. Mol. Biol. 97: 40–
1010 52.

1011 Walter, A., U. Korth, M. Hilgert, J. Hartmann, O. Weichel *et al.*, 2004 Glycerophosphocholine is elevated
1012 in cerebrospinal fluid of Alzheimer patients. Neurobiol. Aging 25: 1299–1303.

1013 Wang, Y., H. Jiang, Y. Cheng, C. An, Y. Chu *et al.*, 2017 Activation of Aedes aegypti prophenoloxidase-
1014 3 and its role in the immune response against entomopathogenic fungus. Insect Mol. Biol. 26: 552.

1015 Will, I., W. C. Beckerson, and C. de Bekker, 2022 Using machine learning to predict protein-protein
1016 interactions between a zombie ant fungus and its carpenter ant host. bioRxiv 2022.09.09.507359.

1017 Will, I., B. Das, T. Trinh, A. Brachmann, R. A. Ohm *et al.*, 2020 Genetic Underpinnings of Host
1018 Manipulation by Ophiocordyceps as Revealed by Comparative Transcriptomics. G3 (Bethesda). 10:
1019 2275–2296.

1020 Yakovlev, I. K., 2018 Effects of Octopamine on Aggressive Behavior in Red Wood Ants. Neurosci.
1021 Behav. Physiol. 2018 483 48: 279–288.

1022 Zheng, S., R. Loreto, P. Smith, A. Patterson, D. Hughes *et al.*, 2019 Specialist and Generalist Fungal
1023 Parasites Induce Distinct Biochemical Changes in the Mandible Muscles of Their Host. Int. J. Mol.
1024 Sci. 20:.
1025 Zhuang, J. X., Y. H. Hu, M. H. Yang, F. J. Liu, L. Qiu *et al.*, 2010 Irreversible Competitive Inhibitory
1026 Kinetics of Cardol Triene on Mushroom Tyrosinase. J. Agric. Food Chem. 58: 12993–12998.
1027